Structure and chemical reactivity of transition metal surfaces as probed by synchrotron radiation core level photoelectron spectroscopy

2008 J. Phys.: Condens. Matter 20 093001

(http://iopscience.iop.org/0953-8984/20/9/093001)

IOP PUBLISHING JOURNAL OF PHYSICS: CONDENSED MATTER

J. Phys.: Condens. Matter **20** (2008) 093001 (19pp) doi:10.1088/0953-8984/20/9/093001

TOPICAL REVIEW

Structure and chemical reactivity of transition metal surfaces as probed by synchrotron radiation core level photoelectron spectroscopy

Alessandro Baraldi

Physics Department and Centre of Excellence for Nanostructured Materials, University of Trieste, Via Valerio 2, I-34127 Trieste, Italy
and
Laboratorio TASC INFM-CNR, S.S. 14 Km 163.5, I-34012 Trieste, Italy

E-mail: alessandro.baraldi@elettra.trieste.it

Received 30 August 2007, in final form 18 December 2007
Published 4 February 2008
Online at stacks.iop.org/JPhysCM/20/093001

Abstract
Since the 1970s core level spectroscopy has played a key role in elucidating the energetics, structure and kinetics of solid surfaces. This paper reviews recent experimental results which illustrate the breakthroughs achieved by using this technique with x-rays produced by third generation synchrotron radiation light sources. Examples regarding the interaction of atomic adsorbates, the role of surface defects, the thermal stability of solid surfaces and simple surface chemical reactions outline the potential of high energy resolution core level photoelectron spectroscopy as a tool for determining electronic, geometrical and chemical properties of clean and adsorbate covered Rh and Pt solid surfaces.

(Some figures in this article are in colour only in the electronic version)

Contents

1. Introduction

In the last 15 years, great research efforts have been devoted by the surface science community to improving the performance of experimental methods, with the aim of gaining deeper insight into the local geometrical and electronic properties of gas–solid interfaces. Besides the obvious interest in understanding the fundamental physical and chemical properties of solid surfaces, one of the ultimate goals is the development of new functional materials with novel properties, e.g. the next generation of nanostructured catalysts. To this purpose, in parallel with the extraordinary development of imaging methods such as scanning tunnelling microscopy (STM), atomic force microscopy (AFM), low energy electron microscopy (LEEM), scanning photoemission microscopy (SPEM), recent advances have pushed forward the limits of conventional spectroscopic methods typically used to probe the electronic and geometrical structure of solid

surfaces. Among the latter methods, core level photoelectron spectroscopy is certainly one of the most commonly used techniques to shed light on the nature of chemical bonds at solid surfaces [1]. Since core levels are quite compact, and do not take part directly in bonds but are affected by them, the changes in core electron binding energies can be used as a local probe of the variation in the electrostatic potential of atoms located in different chemical and geometrical environments, reflecting the variations in their chemical properties [2]. In contrast with other spectroscopic methods commonly used to investigate gas–surface interfaces, such as infrared absorption spectroscopy (IRAS) and high resolution electron energy loss spectroscopy (HREELS) [3, 4], core level spectroscopy is equally sensitive to the binding energy changes of both the adsorbate and substrate atoms. This offers the possibility to use a spatially averaged experimental technique to obtain information about the local electronic structure of surface atoms with different geometrical and chemical coordination.

The advent of third generation synchrotron light sources such as ALS (Berkley, USA), MaxLAB (Lund, Sweden), SLS (Villigen PSI, Switzerland), BESSY (Berlin, Germany) and ELETTRA (Trieste, Italy) has significantly advanced the investigation of gas–surface interfaces and has triggered a new class of core level photoelectron spectroscopy experiments [5–7] exploiting the extraordinary properties of the soft x-ray radiation produced in these facilities: energy resolution down to the 20 meV range [8], high brilliance, which yields an increase of almost three orders of magnitude in flux at the sample with respect to conventional anode based sources, and an enhanced surface sensitivity and photoemission cross section due to photon energy tunability. Complementary theoretical analysis of core level binding energies, often performed within the density functional theory [9, 10] or using *ab initio* self-consistent field Hartree–Fock wavefunctions for atomic clusters [11], are found to reproduce with high accuracy both the trends and the magnitude of the experimental binding energy shifts and are widely used to discuss the origin of the different contributions to the measured core level components.

This article does not intend to provide a comprehensive review of this subject, but instead to give a personal view of the recent progress obtained by using high energy resolution core level spectroscopy with synchrotron radiation in the study of a number of phenomena occurring on clean and adsorbate covered solid surfaces. The results will be described considering the new insights into the nature of the chemical bond, the electronic structure and the surface reactivity provided by experiments performed on single crystal rhodium- and platinum based surfaces, which have been used as prototypical model systems. These transition metals (TM) are the major active constituents of a large range of materials used in heterogeneous catalysis.

Among the catalysts used in car exhaust gas purification via the $2NO + 2CO \rightarrow N_2 + 2CO_2$ reaction, Rh exhibits high activity and excellent selectivity towards N_2 production. Moreover, Rh is a transition metal relevant for the formation of cyanide intermediates [12, 13] and in the formation of N_2O [14], a gas which contributes to ozone layer depletion and to the greenhouse effect [15]. Platinum is among the noble metals that dissociate O_2 molecules and is therefore an efficient oxidation catalyst. Deposited on silica it is used in the production of sulfuric acid, in the cracking of petroleum products and in the conversion of methyl alcohol vapours into formaldehyde [16]. Recently Pt has attracted increased attention in the development of Pt based fuel cell-powered systems [17]: in this case Pt is used for oxidation and/or methanation of CO, sometimes in the form of bimetallic alloys with Ru [18].

The paper is organized as follows. In the next section I discuss the interaction with the surface of atomic adsorbates relevant in catalysis, with particular emphasis on oxygen, nitrogen, sulfur and hydrogen; section 3 contains a description of the synchrotron radiation results concerning the formation of surface Rh oxides. The investigation of surface defects such as steps and highly under-coordinated atoms, like adatoms and dimers, will be described in section 4, while the possibility to tune the CO dissociation reaction probability with artificially constructed nanostructured Rh surfaces is examined in section 5. The electronic structure and the thermal stability of missing row reconstructed Rh surfaces, probed by real-time photoelectron spectroscopy, are considered in section 6. The monitoring of the first layer surface composition of bimetallic Pt–Rh catalysts during a chemical reaction is outlined in section 7.

The concluding remarks emphasize future developments in this field, in particular concerning the improvements of data acquisition speed and enhanced surface sensitivity to probe transition metal nanoclusters deposited on supports.

2. The interaction of atomic species with solid surfaces

Surface science has proven that a multiple experimental techniques approach, paralleled by theoretical calculations, is often needed to obtain a complete picture of the gas–solid surface interface systems under investigation. Ideally, to reach a thorough understanding of these phenomena, one would like to obtain chemical sensitivity at the atomic length scale for both atomic and molecular species and on the timescales of elementary kinetic surface processes. Both are challenging tasks.

Indeed the low sensitivity of vibrational techniques such as HREELS and IRAS to catalytically relevant atomic adsorbates, imposes severe limits to the quantitative chemical determination of atomic species, which are fundamental participants in a large variety of chemical reactions. Furthermore, these experimental methods, which are among the best methods to probe the molecular interactions in complex model systems [19, 20], lack sensitivity to the electronic structure modifications of the first layer atoms induced by molecular and/or atomic adsorption. This impedes the simultaneous detection, identification and characterization of the geometric and electronic structure modifications of the catalyst's first atomic layer during chemical reactions, which are a prerequisite for the understanding of the reaction mechanisms. In this respect, the contribution of high energy resolution x-ray core level spectroscopy has been relevant

since the first experiments on polycrystalline solid surfaces in 1973 [21, 22].

The ability to distinguish the adsorption sites of molecules chemisorbed on long range ordered solid surfaces dates back to the seventies when the group of D Menzel was the first to make quantitative use of adsorbate x-ray photoelectron spectroscopy (XPS) on single crystal surfaces, to disentangle different C 1s core level components originating from CO molecules adsorbed on different sites on W(110) [23, 24]. After those pioneering experiments, XPS was extensively applied on transition metal surfaces to probe the molecular bonding configuration of adsorbed layers, such as CO on Ni(100) [25, 26], Pt(111) [27, 28], Pd(111) [29], Rh(111) [30, 31] and NO on Rh(110) [32] and Pt(111) [33]. As first pointed out by Mårtensson and Nilsson [34] the core level binding energy (BE) shifts of molecular systems can be understood on the basis of total energy considerations, the major contribution arising from the changes in the energy of the core ionized state. For example, it was found for a large number of carbon monoxide adsorption systems that the O 1s BE decreases with increasing CO coordination to the substrate, in the order BE(on-top) > BE(bridge) > BE(hollow), in the range 530.5–531.6 eV, too large to be explained just in terms of initial state effects.

The situation is rather different when atomic species are involved in processes at the gas–solid surface interface: in this case core levels are not always the best tool to determine the adsorption site of these atomic species. Adsorbates such as O, N and S are often located in the same adsorption site and their 1s or 2p levels are not very sensitive to the variations in the adsorbate–metal bond or to adsorbate–adsorbate interactions. For example the O 1s core level BE of O/Rh(111) [35] and O/Ru($10\bar{1}0$) [36], varies from low to saturation coverage, by only −110 and 75 meV, respectively. Following a different approach, high energy resolution photoelectron spectroscopy with synchrotron radiation can be used to probe the shifts of the *substrate* core levels induced by the adsorbed atomic species, offering the unique possibility to identify in a direct way the atomic adsorption sites and to evaluate the changes in the local environment of the substrate atoms. Indeed the core level binding energies of the first layer atoms are not the same as in the bulk, giving rise to so-called surface core level shifts (SCLS) [37], which can be measured with high precision for both clean and adsorbate covered surfaces by combining the high energy resolution of modern electron energy analysers with the use of soft x-ray monochromator based beamlines. In parallel surface core level binding energy shifts can be calculated with a high level of accuracy using DFT, as a total energy difference of the neutral and the core ionized final state [5]. The comparison between experimental and theoretical results is a key ingredient to obtain an unambiguous determination of the geometrical and chemical environment of atomic and molecular species at solid surfaces.

SCLSs usually range from a few meV to more than 1 eV and arise from two contributions: an initial state effect, which reflects the changes at the surface in the electronic distribution of the neutral system before the excitation, and final state effects, originating from the screening of the core–hole created

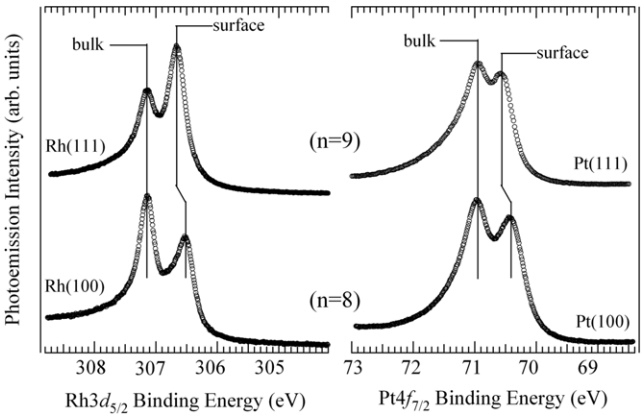

Figure 1. Rh $3d_{5/2}$ (left) and Pt $4f_{7/2}$ (right) core level spectra corresponding to (100) (bottom) and (111) (top) surfaces. By decreasing the first layer atomic coordination n the surface core level shift increases by about 36%, as predicted by the tight-binding model.

at the surface and in the bulk. Initial state effects on clean TM such as Rh and Pt are mainly due to the reduced coordination of the surface atoms with respect to the bulk, which results in a narrowing of the surface d band around its centroid. The d band is electrostatically shifted in order to keep surface and bulk atoms at the same chemical potential, thus moving surface components towards lower binding energy for d bands which are more than half filled, as for rhodium and platinum [38]. Figure 1 shows Rh $3d_{5/2}$ and Pt $4f_{7/2}$ core levels of Rh and Pt (100) and (111) surfaces, with first layer atom coordination n equal to 9 (FCC(111)) and 8 (FCC(100)). The d band narrowing is determined by the number of broken bonds with respect to the bulk of the top layer atoms, which are 3 and 4 for the (111) and (100) surfaces, respectively.

The small energy differences which have to be measured call for a resolution smaller than 100 meV, typically in the photon energy range between 100 and 500 eV, where the shallow $3d_{5/2}$ core levels of 4d TM (such as Rh) or $4f_{7/2}$ core levels of 5d TM (such as Pt) are found. These experimental requirements can be fulfilled only by using the tunable wavelength x-ray beam produced by undulator based synchrotron radiation light sources. As a further advantage with respect to conventional Al or Mg Kα x-ray sources, enhanced sensitivity to first layer atoms can be achieved by maximizing the overall cross sections and minimizing the inelastic electron mean free path.

In the following I will illustrate: (i) how high resolution core level photoemission can be used to identify in a direct way the adsorption sites of different atomic adsorbates on Rh surfaces, (ii) how the modifications in the electronic structure of adsorbate–substrate complexes, monitored at different coverages, can be correlated with the changes of chemical reactivity via the shift of the d band centre, and (iii) the importance of including the contribution of second layer atoms to accurately disentangle the different core level components.

2.1. O, N and S adsorption on Rh(100)

Oxygen, nitrogen and sulfur are light atomic species involved in a well number of chemical reactions and their interaction

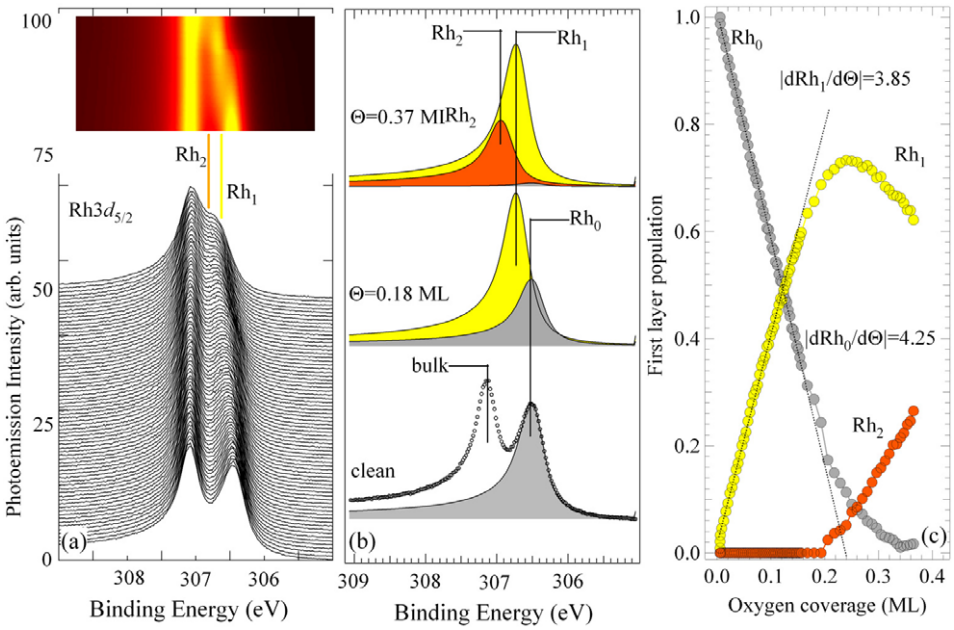

Figure 2. Evolution of the Rh $3d_{5/2}$ core level spectra during oxygen uptake on Rh(100) ($T = 300$ K, $h\nu = 380$ eV), shown as sequence of spectra (bottom) and two-dimensional image (top), Rh_1 (orange) and Rh_2 (yellow) lines are a guide to the eye to show the development of intensity changes at particular binding energies. (b) Rh $3d_{5/2}$ core level components as obtained from the fits of the spectra measured at oxygen coverage of 0, 0.18 and 0.37 ML. The Rh_0 component originates from the clean surface atom, while the Rh_1 and Rh_2 peaks originate from the surface Rh atoms single and double bonded to oxygen. (c) Oxygen coverage dependent intensity of the three components, as obtained by fitting the spectra reported in (a).

with Rh surfaces strongly influence different factors that control catalytic activity and selectivity.

Besides its importance as an archetypal model, the relevance of the oxygen interaction with Rh is connected to its importance in catalytic CO oxidation, as a product in nitric oxide dissociation and in the first step of surface oxide formation (see section 3) [39]. The oxygen–Rh bond can be understood in terms of a strong covalent bond between the O 2p orbital and the metal d band, which is paralleled by a considerable charge transfer from the metal substrate to the electronegative adspecies. The charge redistribution in the valence band results in a modification of the core level binding energy of the surface atoms.

Extensive real-time measurements of the Rh 3d core level have been performed in order to understand the evolution of the local configuration of the oxygen atoms, along with the variations of the electronic structure of the substrate Rh atoms.

Figures 2(a) shows a sequence of Rh $3d_{5/2}$ spectra measured at different coverages during oxygen exposure at room temperature [40].

As previously reported in figure 1, the Rh $3d_{5/2}$ spectrum corresponding to the clean (1×1) Rh(100) surface is composed of two main peaks [5, 41]: the higher binding energy component at 307.15 eV, Rh_{bulk}, originating from the second and deeper layers, and the lower binding energy peak at -660 meV from Rh_{bulk}, Rh_0, due to the topmost Rh atoms.

In order to evaluate the position and the intensity of the different oxygen-induced surface core level shifted components, a fit of the spectra has been performed using Doniach–Šunjić (DS) function [42] convoluted with a Gaussian. The DS function is the line shape which is commonly used to fit the core level spectra of solids, such as beryllium [8, 43], alkali [44] and TM [5, 41, 45].

All the spectra in the uptake series in figure 2(a) can be accurately fitted using only the bulk and surface peaks and two additional components. Distinct modulation features are visible in the two-dimensional image (top panel in figure 2(a)) which shows, in a two-dimensional colour scale, the spectral changes occurring during the uptake process. Oxygen adsorption at low coverage leads to the appearance of a new core level component Rh_1 shifted by -425 ± 20 meV with respect to the bulk peak (the yellow component in figure 2(b)), while the original Rh_0 surface peak intensity decreases. Upon increasing the surface coverage, a further decrease of the Rh_0 component is observed, accompanied by the growth of a third surface component Rh_2 at a binding energy of -210 ± 20 meV (orange component in figure 2(b)): this process takes place simultaneously with the p(2 × 2) to c(2 × 2) structural conversion observed by means of spot profile analysis low energy electron diffraction measurements [40, 46]. The intensity variation of the different core level components, as obtained from the analysis of the whole data set, is plotted in figure 2(c) against the oxygen coverage. For coverages below 0.1 ML, oxygen adsorption induces a linear decrease of the Rh_0 component, which disappears slightly above 0.3 ML. The first derivative $\mathrm{d}\,Rh_0/\mathrm{d}\Theta$ calculated for low coverage is equal to -4.2, thus indicating in a direct way that for each oxygen atom adsorbed on the surface, the intensity contribution of about four surface Rh atoms moves from Rh_0 to Rh_1. The initial adsorption site for oxygen is confirmed to be fourfold, as previously determined by LEED measurements [47, 48]. The Rh_1 component therefore originates from first layer rhodium

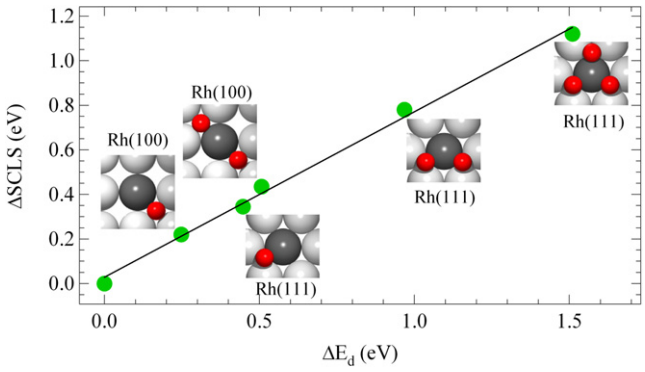

Figure 3. Core level shift variations for first layer Rh atoms in different local environment on both (100) and (111) surfaces, versus the calculated atom-projected d band shift. The shifts are measured with respect to the clean surface component.

atoms bonded to a single oxygen atom, while the Rh_2 peak, which grows at coverages larger than ∼0.2 ML, is due to Rh atoms bonded to two oxygen atoms.

It is important to note that the adsorption site assignment is based on the behaviour of the intensity of the Rh_0 component alone, while the absolute intensity ratio between the different components may not reflect the true occupancy of the adsorption sites. Differences can be caused by strong photoelectron diffraction effects [49], due to the inequivalent local surrounding of the Rh atoms that are differently coordinated with oxygen. Indeed these effects are so strong that they can be used in a straightforward way to verify the chemical assignment of measured core level shifted components [50–52].

Further important information provided by these experiments concerns the changes in the local electronic structure, measured by the variation of the binding energy ΔE of atoms in different chemical environments (Rh_1 and Rh_2) with respect to the clean component Rh_0, which can be experimentally determined with great accuracy. Indeed, since $\Delta E_1 = +220$ meV and $\Delta E_2 = +435$ meV, it turns out that $\Delta E_1 \cong 2\Delta E_2$. The same experiment, repeated on the Rh(111) substrate demonstrates the validity of the additivity property of the oxygen-induced Rh energy shift caused by the individual fractional contribution of adsorbates [53].

The changes of CLS of Rh atoms bonded with oxygen atoms in different configurations are plotted in figure 3 against the calculated atom-projected shift of the d band centre. The linear behaviour unambiguously proves that the variation of the CLS is strongly correlated with the changes of the d band centre position, which is directly related to the chemical reactivity of d metal surface atoms. However, this interpretation is based solely on an initial state picture of the SCLS, i.e. the difference in the single energy eigenvalues of a surface and a bulk atom core state. This approach neglects therefore the different contribution of surface and bulk valence electrons for screening the core hole. Nevertheless, final state effects, which can make a substantial contribution to the shifts in the case of surface alloys [54], are of minor relevance for Rh.

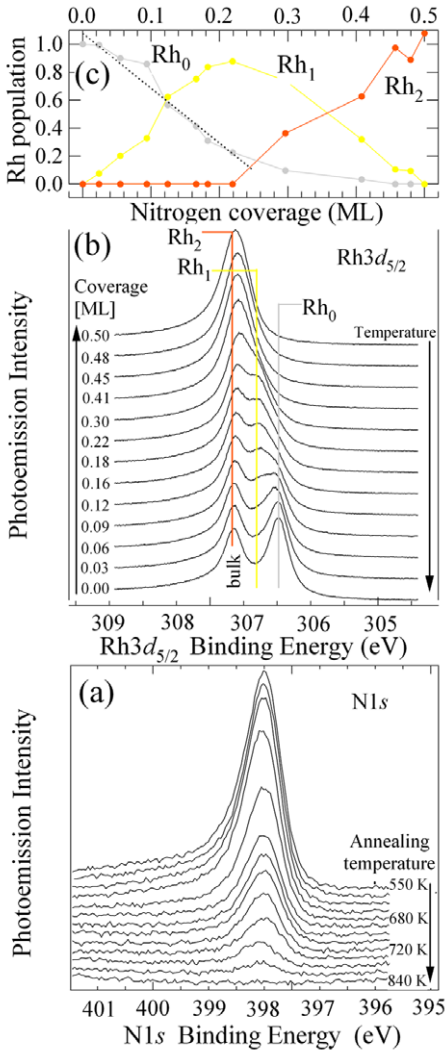

Figure 4. (a) N 1s core level spectra measured at 100 K ($h\nu = 470$ eV), corresponding to adsorbed layers with different coverage, obtained by annealing the c(2 × 2) saturated surface to progressively higher temperature. (b) Rh $3d_{5/2}$ core level spectra corresponding to the same layers (N coverage is indicated) ($h\nu = 400$ eV). (c) Intensity evolution of the Rh_0, Rh_1 and Rh_2 components, which correspond to surface Rh atoms respectively clean, single and double bonded to N atoms. The first derivative of the Rh_0 component is also reported.

A similar experimental approach has been used to study the interaction of atomic nitrogen on Rh(100), supported by first-principles theoretical calculations of the surface core level and d band energy shifts [55]. The major interest in nitrogen adsorption on transition metals is connected with the catalytic synthesis of ammonia from N_2, while for group VIII metals like Rh, N_2 formation is extremely important as a subsequent reaction step in NO and NH_3 molecular dissociation.

In order to determine the changes in the local nitrogen–Rh configuration along with the variations in the first layer Rh electronic structure, the Rh $3d_{5/2}$ core level spectra, reported in figure 4(b), have been measured as a function of the nitrogen coverage which has been determined by evaluation of the intensity of the N 1s spectra (figure 4(a)).

The evolution of the spectral line shape is quite similar to that found for the O–Rh(100) system. In particular, a component shifted by -360 ± 20 meV with respect to the bulk peak, grows with N coverage between the bulk and the clean Rh_0 peak while the clean surface peak intensity decreases. Upon further increase of the N coverage, a new component Rh_2, very close in energy to the bulk peak, at $+10 \pm 30$ meV, had to be included in the fit. The integrated intensity of the different surface core level components is reported in figure 4(c). The first derivative of the Rh_0 components is equal to -3.9 ± 0.4, thus indicating that the adsorption site is fourfold hollow, in agreement with theory [56]. The Rh_1 and Rh_2 components originate from first layer Rh atoms single and double bonded with nitrogen.

In order to obtain a deeper understanding of the measured values of the SCLS, theoretical calculations based on DFT [57, 58] and using the local density approximation [59–61] have been performed. The nitrogen overlayers corresponding to different coverages were modelled, with the N atom always adsorbed in the fourfold hollow site.

The results of the theoretical calculations of the SCLS, reported in the right side of figure 5, clearly indicate that there is a strong dependence of the SCLS on the Rh atom–adsorbate coordination, as shown in section 2.1 for the oxygen case. As outlined above, the SCLS of second layer atoms, ranging from -103 to $+159$ meV makes it difficult to consider them in the spectral fitting procedure. As for the O–Rh(100) system, a close comparison with the experimental results takes into consideration the ΔE_i shifts of the nitrogen-induced SCLSs R_i $(i = 1, 2)$ with respect to the clean Rh_0 component. The experimental values of $\Delta E_1 = 300 \pm 40$ meV and $\Delta E_2 = 670 \pm 60$ meV are in quite good agreement with the theoretical ones and indicate that even for the N–Rh(100) systems, the $\Delta E_2 = 2\Delta E_1$ relation holds.

While the shift towards higher binding energy with increasing N coverage can be qualitatively understood as due to charge transfer from the surface to the adsorbate, the quantitative determination of the shift cannot be accounted for by charge transfer arguments only, as expected for the adsorption of electronegative species on 4d transition metals surfaces.

What was found for the N–Rh(100) case is a strong correlation between the ΔE values and the valence d band shift projected onto the surface atoms. The calculated density of states (DOS) per atom, projected onto the 4d orbitals of surface, bulk and first layer Rh_1 and Rh_2 atoms coordinated with nitrogen, is plotted in figure 5. The nitrogen adsorption clearly induces a broadening of the Rh d band, along with a lowering of the DOS in the Fermi level region. This results in a d band centre B_d shift towards higher binding energies with increasing nitrogen coverage. The variation of d band centre with respect to the bulk values (ΔB_d) ranges from negative values for the clean first layer atoms Rh_0 (-578 meV) to more positive values in the case of Rh_1 (-391 meV) and Rh_2 (-70 meV).

The major interest in applying the surface core level shift approach to sulfur chemisorbed on Rh(100) resides in the well known, extensively studied poisoning effect

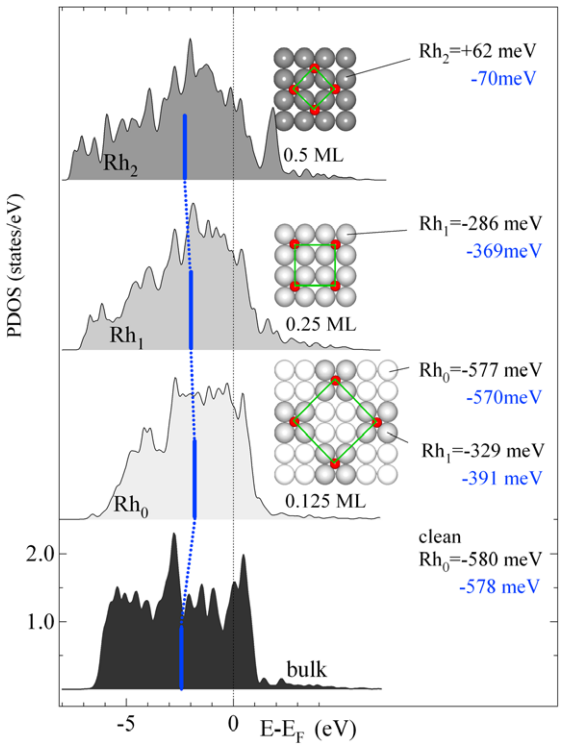

Figure 5. Density of states projected onto the 4d orbitals of the Rh atoms for all the inequivalent surface atoms at the three studied coverages, corresponding to the $p(2\sqrt{2} \times \sqrt{2})$—0.125 ML, $p(2 \times 2)$—0.25 ML and $c(2 \times 2)$—0.5 ML nitrogen ordered structures. Bottom panel corresponds to Rh bulk atoms. Rh_0, Rh_1 and Rh_2 are Rh atoms bound to 0, 1 and 2 nitrogen atoms, respectively. On the right side, final state SCLS values for the inequivalent atoms are reported in black, while the displacement ΔB_d of the d band average energy with respect to the bulk value is indicated below (blue).

of this adsorbate [62, 63]. Indeed the presence of S in natural hydrocarbon sources causes a strong reduction of the lifetime and performance of Rh based catalysts. By analysing the rate of CO methanation as a function of S coverage on Rh, Ru [64, 65] and Ni [66, 67], it was found that methanation rate and sulfur coverage do not follow a linear relationship, and a sharp decrease in the catalytic activity was observed already at low sulfur coverage. It was suggested that a single sulfur atom may change the electronic structure in a surface area with a radius of about 10 Å, reducing the catalytic activity of the area through a long range electronic effect [68]. This was confirmed by theoretical calculations which have shown that electronegative atoms induce a reduction of the DOS near the Fermi level, that can extend beyond next nearest neighbours [69, 70]. Since recent theoretical calculations [71–74] have attributed instead the S-induced reduction in the chemical reactivity of Rh and Pt to the poisoning of highly surface reactive defects such as steps, S–Rh(100) appears to be the ideal system to investigate with a probe highly sensitive to the local electronic structure, such as high energy resolution core level photoelectron spectroscopy [75].

A sequence of Rh $3d_{5/2}$ core level spectra measured at different sulfur coverages is reported in figure 6. Below 0.2 ML

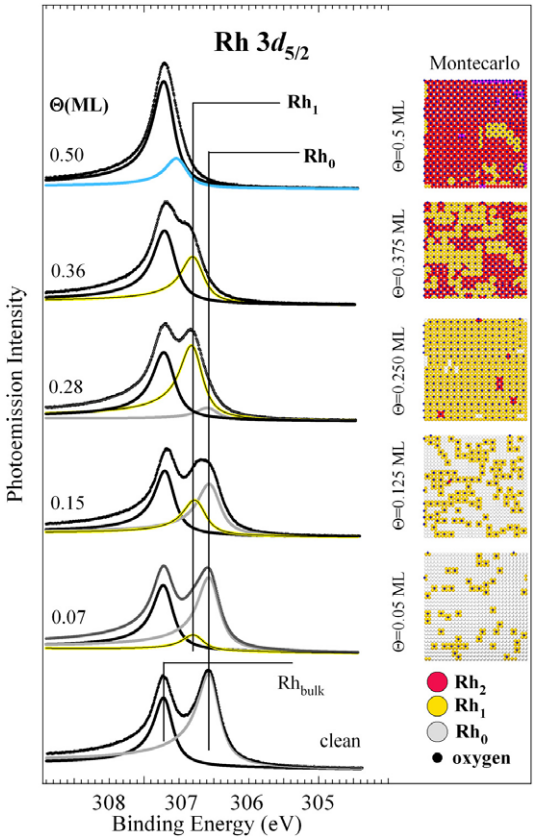

Figure 6. Rh $3d_{5/2}$ core level spectra from S–Rh(100) measured at increasing coverage and at $T = 100$ K with 400 eV photon energy. Different spectral components corresponding to different Rh local configurations are also shown with different colours. On the right, snapshot structures of sulfur distribution on Rh(100) as obtained in the MC simulations using the UBU-QEP model at coverages ranging from 0.05 to 0.5 ML, are reported. Grey atoms correspond to clean first layer Rh atoms (Rh_0), yellow atoms correspond to first layer Rh atoms single bonded with S (Rh_1), red atoms to first layer Rh atoms double bonded with S (Rh_2). A minority population of Rh atoms triple bonded with S is shown in violet at 0.5 ML in the MC simulations.

the Rh_1 component grows at higher binding energy with respect to the Rh_0 surface peak (SCLS $= -440 \pm 20$ meV). At higher coverage the increase of Rh_1 is accompanied by a strong decrease of the Rh_0 peak, while at larger S coverage a third component (SCLS -240 ± 20 meV) is required to accurately fit the data. By comparing the sulfur-induced Rh $3d_{5/2}$ line shape changes with the O- and N-induced spectral variations, it is straightforward to attribute the third component to first layer Rh atoms double bonded with S atoms. However this interpretation does not account for the high spectral intensity in the bulk region, at about 307.2 eV, revealed by the analysis of the 0.5 ML spectrum.

Indeed the S-induced Rh $3d_{5/2}$ surface core level shifts, calculated using the same formalism adopted for the nitrogen case, indicates that Rh_2 atoms produce a SCLS of +22 meV, which cannot be experimentally distinguished from the bulk peak. The origin of the component measured at −240 meV can be found in an unexpectedly large contribution of second layer atoms. The theoretical analysis in fact predicts for the atoms sitting in fourfold sites just below the first layer S atoms, a second layer core level shift equal to −235 meV, which has two origins: a large expansion of the first inter-layer distance and a substantial electronic charge redistribution also in the second layer, induced by the S adsorption.

The most relevant result of this investigation is connected to the S-poisoning effect. DFT calculations for the low coverage S structure do not report a significant variation in Rh_0 SCLS and d band centre shifts, which exclude a S-induced long range effect on the electronic structure of the next nearest neighbour Rh atoms.

This necessitates an alternative interpretation of the S-induced poisoning effect, which has to be related to the site blocking effect exerted by sulfur when it strongly chemisorbs on the catalytically active sites of Rh surfaces, e.g. kinks and steps.

From the theoretical calculations it was found that, in contrast to the O– and N–Rh(100) systems, the $\Delta E_2 = 2\Delta E_1$ relation does not hold for S–Rh(100). This is due to the large screening contribution (+162 meV) to the CLS of the Rh_2 atoms of the c(2 × 2) structure, while for other different Rh configurations the absolute value of the final state contribution remains usually below 100 meV.

These results confirm the paramount importance in interpreting core level binding energy shifts of the interplay between experiments and theory, which can take into account the final state effects due to the different screening capabilities of the core ionized system at the surface and in the bulk. Moreover the theoretical results have provided new insights into the important role of sub-surface species: second layer contributions to core level spectra can indeed be relevant and an assignment based exclusively on peak intensities could be misleading due to photoelectron diffraction effects.

The selected examples of interaction of atomic species with Rh(100) show that measurements of adspecies-induced SCLS is a solid experimental approach which can go on with the investigation of more complex model catalysts. Although the use of single crystals and the minimum number of adspecies are substantial simplification for the understanding of the adsorbate–surface interaction properties, the technique is mature to be extended to the investigation of two or more coadsorbed atomic and/or molecular species or to the analysis of the kinetics of simple chemical reactions where atomic species play a relevant role.

2.2. Hydrogen on Rh(100)

One of the most remarkable results obtained by surface core level shift methods in the study of atomic adsorbates is the determination of the hydrogen adsorption sites on solid surfaces [76, 77]. Even if in a number of cases diffraction and spectroscopy based techniques have been successfully applied to unravel the H–metal bond configuration [78, 79], this remains in general a difficult problem because of the low hydrogen scattering cross section and the high surface mobility of hydrogen atoms. However, following an alternative approach based on the measurement of the hydrogen-induced Rh $3d_{5/2}$ surface core level shift, it was possible to probe

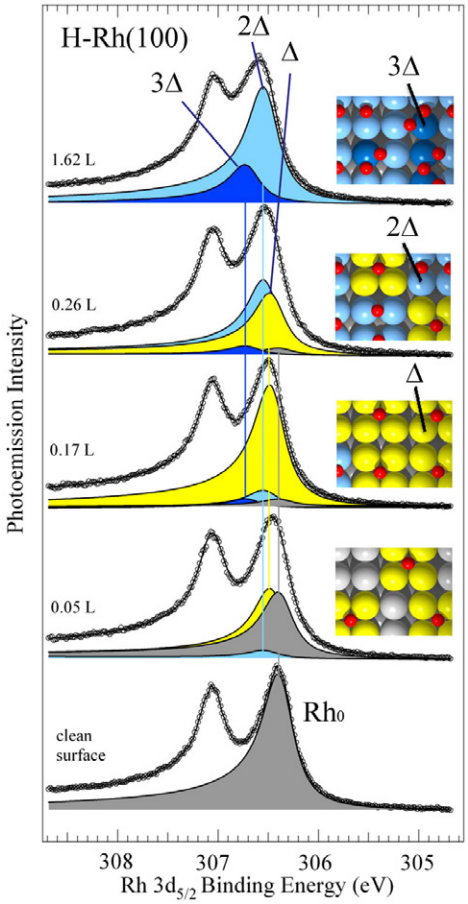

Figure 7. Selected Rh $3d_{5/2}$ core level spectra measured during hydrogen uptake on Rh(100) at 150 K. Photon energy: 407 eV. Different contributions (Δ, 2Δ, 3Δ) shown using different colours are due to differently hydrogen-coordinated first layer Rh atoms, as shown in the geometrical models. In all spectra the bulk component is omitted.

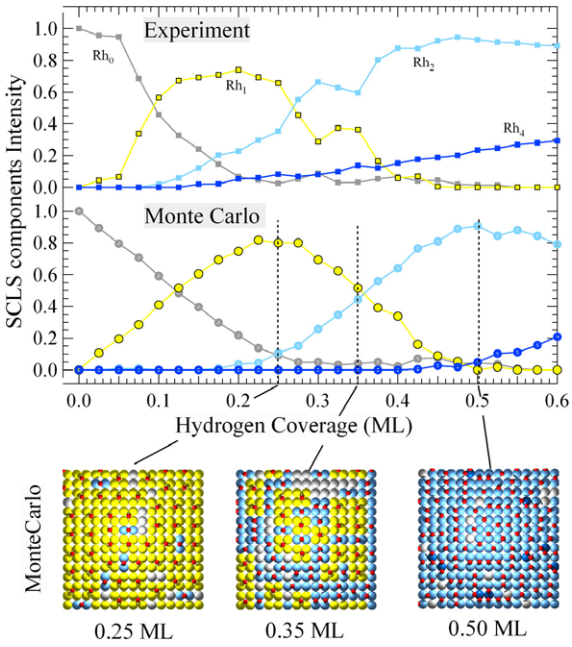

Figure 8. Experimental and simulated curves for the intensity of the surface core level shifted components assigned to inequivalent first layer Rh atoms. The grey component Rh_0 originates from clean surface Rh atoms, while the yellow Rh_1 and light blue Rh_2 components originate from surface Rh atoms which bind to one hydrogen atom in fourfold hollow sites and in bridge sites (Rh_4), respectively. First layer Rh atoms bonded to two hydrogen atoms sitting in bridge sites are reported in blue. Snapshot structural models of the equilibrium configurations as obtained by Monte Carlo simulations during hydrogen uptake.

the hydrogen occupation of both fourfold hollow and bridge adsorption sites on Rh(100) [76].

The core level spectra reported in figure 7, and measured during hydrogen uptake at 70 K, show (besides the bulk and surface peaks) the presence of three additional components, due to the H interaction with the surface. The best fit of the whole series was obtained using three components shifted by −545 (yellow, Δ), −480 (light blue, 2Δ) and −310 (blue, 3Δ) meV from the bulk peak respectively, which grow with increasing hydrogen exposures. By measuring the shift with respect to the clean surface peak, as for the O–, N– and S–Rh(100) systems, the new features appear at +80 (Δ), 145 (∼2Δ) and 315 (∼4Δ) meV.

Based on the same model previously applied to other adsorbates, the feature at Δ meV can be interpreted as due to surface Rh atoms bound to a single hydrogen atom adsorbed in a fourfold hollow site. With the same considerations, the 2Δ meV peak can be attributed to Rh atoms bound with either two H atoms in hollow sites or to a single H atom placed in bridge position. The largest shift can finally be associated with Rh atoms coordinated either to four hydrogen atoms in fourfold hollow position or to two H atoms in bridge sites, since the on-top position, which would also be compatible with the model, is strongly unfavoured energetically.

In order to describe the evolution of the surface layer during the H uptake, to link the variations to the observed surface core level components and to distinguish between the possible atomistic configurations, Monte Carlo simulations [80, 81] have been carried out. The experimental and simulated coverage evolution of the differently coordinated first layer Rh atoms, are in very good agreement, as shown in figure 8.

As for the O–Rh system, the Rh $3d_{5/2}$ peak positions measured with respect to the clean surface component on Rh(111) and Rh(100), and associated with the surface species bonded with H atoms in inequivalent configurations (threefold hollow, fourfold hollow and bridge), shows a remarkable linear trend, as reported in figure 9.

The major drawback of using the SCLS approach to study the H interaction with TM surfaces is the small shift induced by H atoms if compared with the changes induced by other adsorbates such as those presented in section 2.1. The difficulty to disentangle differently shifted components makes a constraint on the application of this technique: only simple systems, such as flat and defect-free surfaces, were successfully probed until now. However a possibility to extend the application of this method can be found in the study of H interaction on ultrathin films (1 or 2 layers) of TM pseudomorphically grown on metal or oxide substrates: here

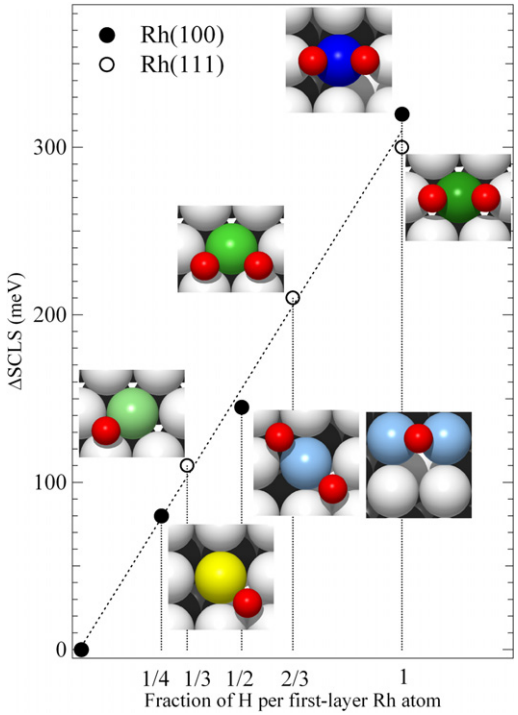

Figure 9. Rh $3d_{5/2}$ core level shift variations for first layer Rh atoms in different local environments on both (100) and (111) surfaces plotted against the number of shared hydrogen atoms per surface Rh atom. The shifts are measured with respect to the clean surface component.

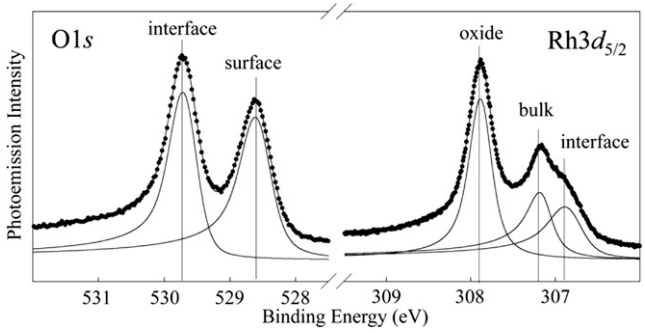

Figure 10. O 1s and Rh $3d_{5/2}$ core level spectra corresponding to the c(2 × 8) structure formed by heavy oxidation of the Rh(100) surface. The O 1s spectrum (left) shows two components of similar intensity, shifted by 1.10 eV and originating from interface and surface oxygen species. The Rh $3d_{5/2}$ spectrum (right) reveals, apart from the bulk peak, two components, corresponding to interface and oxide species, respectively.

higher accuracy in the determination of the H-induced core level components can be easily reached thanks to the absence of bulk components.

3. The formation of surface oxides

Significant experimental and theoretical research work has focused in the last few years on the initial oxidation of TM surfaces, motivated by the importance of this process in technological applications such insulating thin films in microelectronics, layers to protect against corrosion, and catalysis.

After the formation of an oxygen chemisorbed layer, the onset of sub-surface penetration often takes place above a critical coverage, as reported for Ag(111) [82]. For other systems, oxygen exposure at high pressure results in the formation of surface oxides with a structure totally different from the corresponding bulk oxides [83] and with a significant increase in the chemical reactivity [84]. The situation is quite complicated in the case of Rh surfaces. Here high energy resolution core level photoelectron spectroscopy, accompanied by complementary information based on STM, surface x-ray surface diffraction and DFT calculations, has provided a significant contribution to understanding Rh surface oxide formation [85, 86].

On Rh(100), high pressure oxygen exposure results in the development of a hexagonal c(8 × 2) LEED pattern, which is a coincidence lattice of two different structures. High energy resolution core level photoemission measurements revealed that the Rh $3d_{5/2}$ core level spectrum, shown in figure 10 (right), is formed by the bulk peak (Rh_b) and two additional components, S and I, shifted by +730 and −320 meV with respect to Rh_b. The higher binding energy component is due to surface Rh atoms highly coordinated by oxygen, while the lower binding energy peak originates from Rh at the interface between the Rh surface and the hexagonal oxide structure. The O 1s core level spectrum of figure 10 (left) shows two components shifted by 1.1 eV and with similar intensities, originating from inequivalent oxygen atoms. Photon energy dependent measurements have unambiguously demonstrated that the higher binding energy component is due to the interface O atoms. The results of the data analysis indicate that the surface oxide has a trilayer RhO_2 structure, very similar to that found on Rh(111) [85]. Close comparison of photoemission results with LEED, STM, surface x-ray diffraction (SXRD) experiments and DFT structural calculations allowed a model for the oxygen-induced c(8 × 2) structure to be constructed, with an in-plane lattice constant of 3.07 Å and with the oxygen atoms at the interface located in the on-top site of the Rh substrate. A further convincing proof of the reliability of this structural model comes from *ab initio* calculations of the core level shifts of the inequivalent oxygen and Rh atoms.

These and other experiments performed on other Rh, Pd, Ag and Pt surfaces provide convincing evidence that core level spectroscopy has played a vital role for probing the different chemical environment of transition metal atoms at surface oxides and to test state-of-the-art theoretical models at the atomic scale. Besides the presence of differently shifted BE components, the technique can provide the chemical composition in terms of oxygen and transition metal relative abundances.

4. Surface defects

There are several highly reactive sites on solid surfaces. Among them steps represent a particular class, where usually a strong reduction of the dissociation energy barrier occurs.

This has been first demonstrated by Ertl's group for NO on Ru(0001) [87]: STM images have shown an enhanced concentration of adsorbed nitrogen atoms near the steps after exposure to NO. The reason of this effect can be found in the reduced coordination of the atoms at the steps which results in a smaller d band width. This, in turns, implies that the d band centre is shifted upwards compared to the other surface metal atoms. According to the Hammer–Nørskov model [88, 89] these atoms, and more generally under-coordinated atoms at solid surfaces, should be able to bind adsorbates more strongly than others. Recent experiments have also shown that steps influence not just the chemical activity, but also the selectivity in reactions involving multiple reaction pathways, as in the case of ethylene decomposition on nickel [90]. Typically the properties of under-coordinated atoms at solid surfaces are investigated my means of microscopy techniques such as STM [91] and field ionization microscopy [92] which are unique tools for resolving the atomic scale structure of surfaces. More recently the under-coordinated atomic configurations have been successfully explored by means of high resolution core level spectroscopy.

4.1. Stepped Rh surfaces

The possibility to identify step Rh atoms has been firstly demonstrated by Gustafson *et al* [93], who have studied the difference in the core level binding energy between flat (111) and vicinal (553) Rh surfaces. The latter is formed by (111) terraces, five atoms wide, separated by monatomic (100) steps.

The Rh $3d_{5/2}$ core level spectrum of the (553) Rh surface, shown in figure 11, was fitted with four components: besides the bulk peak at higher binding energy, the spectrum shows two other components at lower binding energy, originating from terrace (T) and step (S) atoms. However, by using just two surface components it is not possible to obtain acceptable fits and a fourth component labelled U, with a binding energy very close to the bulk peak, had to be added. Photon energy scans were taken in order to understand the origin of the U component, which was finally assigned to the atoms underneath the (100) steps.

The binding energy shifts of the S, T and U components vary almost linearly with the respective coordination number, even if the T component differs among different vicinal surfaces. This was attributed to in-plane relaxation on the terraces of the vicinal surface due to different tensile stress on (553) and (15 15 13) surfaces, which can induce small core level binding energy shifts.

The higher reactivity of stepped surfaces was finally demonstrated by the analysis of the different core level components after exposing the surface to small amounts of oxygen at room temperature. The comparison of the Rh $3d_{5/2}$ spectra corresponding to clean and adsorbate covered surfaces shows that changes in the S and T components are consistent with oxygen atoms occupying every second of the threefold hollow sites along the steps formed by two S atoms and one T atom.

This experiment has shown that core level spectroscopy can provide a direct observation of the active sites in a catalytic material. This finding opens up the possibility to study interesting kinetic processes at step atoms.

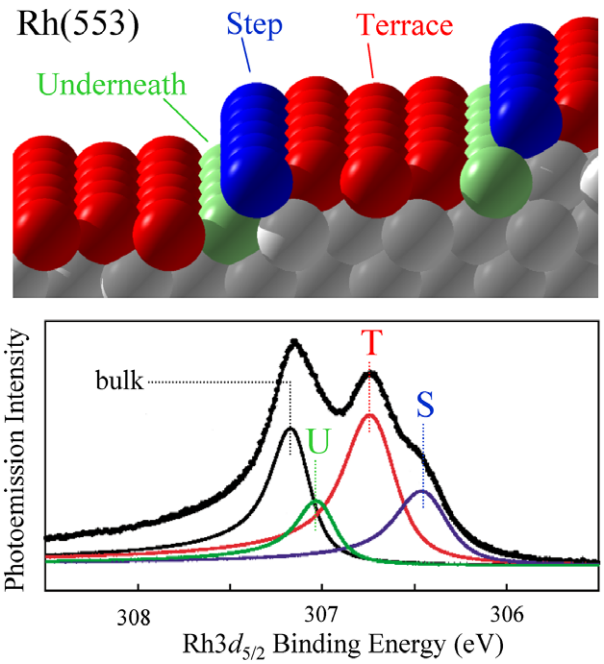

Figure 11. Rh $3d_{5/2}$ core level spectrum from the Rh(553) surface. The surface components S, T and U originate from differently coordinated first layer atoms sitting on the (111) terraces (T—red), on the steps—(100) microfacets—(S—blue) and underneath the step (U—green), as shown in the upper panel.

4.2. Rh adatoms and ad-dimers on Rh surfaces

More recently, the interest in the electronic structure of atoms in special sites on Rh surfaces has been extended to highly under-coordinated atoms, such as adatoms and ad-dimers, which can exist in appreciable concentrations at elevated temperatures because of the evaporation from kink sites at steps [94, 95]. Spectral components originating from atoms with several different coordination numbers, i.e. with the nearest neighbour number n equal to 3, 4 and 5, have been detected by measuring the core level shift induced by Rh adatoms and ad-dimers adsorbed on the (100) and (111) Rh surfaces at low temperature ($T = 20$ K) [96].

The Rh $3d_{5/2}$ spectrum, reported in figure 12, corresponding to a low coverage (0.035 ML) of Rh adatoms deposited on Rh(100) can be fitted using the bulk and surface components used for the (1×1) clean surface, and two additional components at -1030 and -400 meV with respect to the bulk peak. These spectral features are assigned to adatoms (yellow atoms with $n = 4$) and to the surface atoms coordinated to the adatoms (blue atoms with $n = 9$), respectively. For larger Rh deposition times, two extra components at -810 and -145 meV have to be included in the fit in order to obtain a residual with negligible structure. The two components are interpreted as due to the formation of ad-dimers ($n = 5$ and $n = 10$).

In order to extend the range of coordination number, Rh adatoms have also been prepared on Rh(111). At an adatom

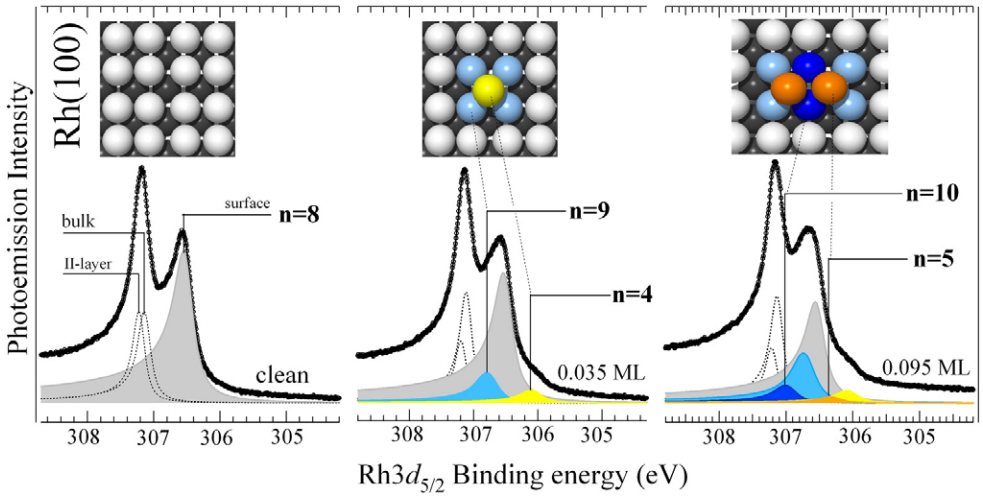

Figure 12. Rh $3d_{5/2}$ core level spectra corresponding to clean (left), 0.035 ML (central) and 0.095 ML (right) Rh covered surfaces. Dashed curves correspond to bulk and second layer atoms, while coloured curves originate from Rh atoms with different coordination.

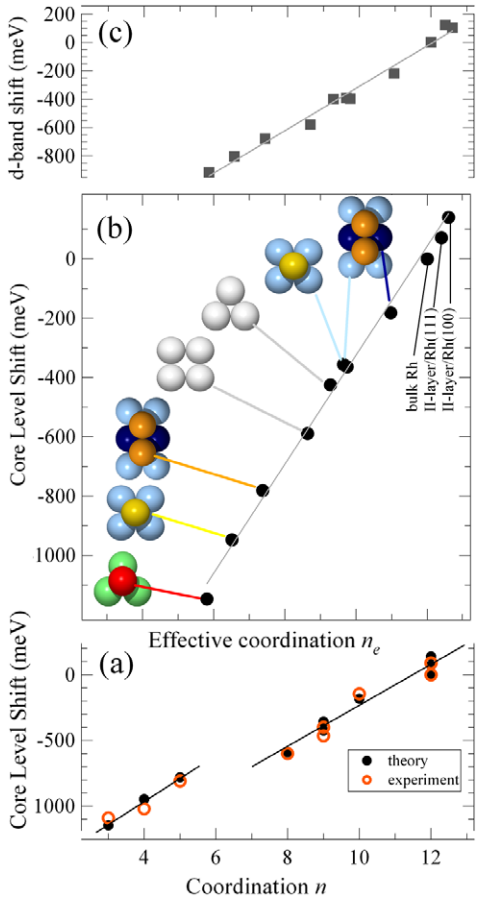

Figure 13. (a) Experimental and calculated Rh $3d_{5/2}$ core level shifts versus the coordination number n. (b) Calculated CLSs versus the effective coordination n_e described in the text. Second layer atoms of Rh(111) and Rh(100) are also included. (c) Linear dependence behaviour of the d band centre binding energy position as a function of the effective coordination number n_e.

coverage of 0.04 ML, a core level component shifted by −1080 meV was found, and attributed to single adatoms with coordination $n = 3$.

The results of the experimental core level shifts from both surfaces are plotted in figure 13(a) as a function of the coordination number, which ranges from 3 to 12.

A quantitative understanding of the origin of the different core level components has been obtained on the basis of DFT calculations, and the agreement between theoretical and experimental results reported in figure 13(a) is remarkably good. Even if the core level shift behaviour follows approximately a linear trend, it is apparent that the low coordination data points are positioned on a different line with respect to the higher coordination data.

This has been explained as due to a strong interplay between the coordination number n and the local bond strain. Indeed calculations found a large relaxation of about −7% taking place at low coordinated adatom and ad-dimers sites, due to the reduced symmetry.

The calculated core level shift data are plotted therefore in figure 13(b) against the effective coordination $n_e(i) = \sum_j \rho^{at}_{Rh}(R_{ij})/\rho^{at}_{Rh}(R_{bulk})$, where the sum is calculated over all the nearest neighbours j of atom i and $\rho^{at}_{Rh}(R)$ is the calculated spherical charge density distribution of an isolated Rh atom as a function of the distance R from the nucleus. R_{ij} is the distance of the j nearest neighbour from the i atom and R_{bulk} the bulk interatomic distance.

The linear behaviour of the CLS versus $n_e(i)$ in the plot integrates the contribution of both the coordination number n and the interatomic distances. Moreover, since the effective coordination is proportional to the calculated d band shift, as shown in figure 13(c), the CLS measurements can be considered, for the systems where final state contributions can be neglected, good spectroscopic fingerprints of the local chemical reactivity. Finally these experiments confirm that core level spectroscopy with synchrotron radiation is a valuable tool to investigate highly under-coordinated configurations of TM atoms, foreshadowing possible applications of this method to the study of nanostructured surfaces as in the case of oxide-supported metal nanoclusters.

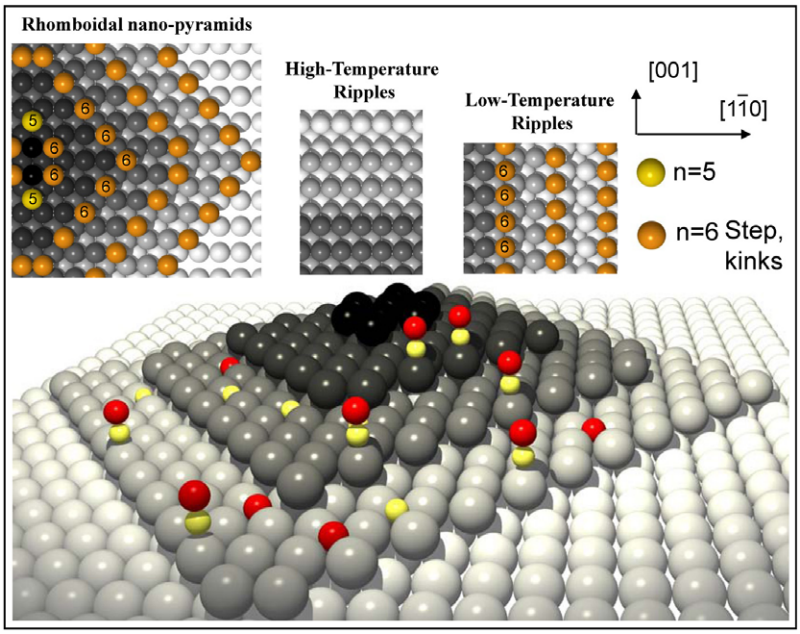

Figure 14. Model for rhomboidal pyramids determined from the SPA-LEED data [101, 102] and for the high temperature ripples and low temperature ripples. Atomic coordination numbers are also reported, with n = number of nearest neighbours.

5. Carbon monoxide dissociation on nanostructured Rh surfaces

Along with the basic interest in understanding the mechanism involved in dissociative adsorption of heteroatomic molecules, CO interaction with transition metal surfaces assumes a significant role in heterogeneous catalysis since the dissociation process is a key step in the syngas and in the Fisher–Tropsch reactions [97].

Experimental and theoretical investigations report that the carbon monoxide chemical reactivity strongly increases on corrugated surfaces and that CO dissociation is sensitive to the structure of the substrate: steps and kinks drastically modify the reaction paths on solid surfaces and appear to be the most active sites for the C–O bond breaking [98, 99]. On Rh, detailed calculations [100] based on DFT report reaction barriers which strongly decrease when passing from the flat Rh(111) surface ($E_a = 1.17$ eV) to steps ($E_a = 0.30$ eV) and kinks ($E_a = 0.21$ eV).

The tuning of the morphology and the step distribution of a Rh(110) surface by controlled irradiation of the surface with a Xe ion beam at a few hundred eV [101, 102] open up the possibility to test and compare with high accuracy the CO catalytic reactivity of non-equilibrium periodic nanostructures such as nanoscale ripples oriented along different crystallographic directions and rhomboidal nanopyramids [103, 104]. A structural model of these nanostructured surfaces, showing the geometry and the under-coordinated step sites, is presented in figure 14.

In order to probe the carbon monoxide decomposition process C 1s and O 1s core level spectra were measured after CO exposure at $T = 200$ K up to saturation. Figure 15(a) shows the evolution of the C 1s spectra measured at 250 K after annealing of the saturated layer at different temperatures. The presence of two components at 286 and 285.55 eV reflects the occupation of two different adsorption sites, which are assigned to CO adsorbed in on-top and bridge sites. Upon a temperature increase, C 1s spectra drastically change: the two components lose intensity due to CO desorption, and a lower binding energy component assigned to atomic carbon and oxygen originating from dissociated CO, grows in intensity at about 283.6 eV. In agreement with experiments performed on defect-free Rh surfaces, on-top CO is the only species present on the surface above 450 K. After heating to 563 K, ~10% of the initial CO has converted into atomic carbon, as shown in figure 15(b). The core level data acquired with an initially lower CO coverage show that when bridge-bonded CO is absent, atomic C still grows, as a product of dissociation of on-top CO. In this case the fraction of dissociated CO after annealing represents 22% of the total CO, i.e. a much larger than the value obtained for the CO saturated layer. The tendency to a higher dissociation probability for a lower initial coverage is confirmed by the results obtained with a very low initial on-top coverage. Because of the high sensitivity of core level spectroscopy it is possible to measure the temperature behaviour of a very low initial coverage, 0.03 ML: here $80 \pm 14\%$ of the molecules undergo dissociation upon surface annealing.

The CO reactivity was probed also for different nanostructures, in particular ripples running along [1–10] (high temperature ripples) and [001] (low temperature ripples), which are endowed with a high density of steps as shown in figure 14. For both structures about 4% of the saturated CO layer undergoes dissociation.

In contrast with the (111), (100) and (110) flat Rh surfaces which present first layer atoms with coordination n equal to 9, 8 and 7 respectively, the rhomboidal nanopyramids are composed of a large number of fivefold and sixfold coordinated

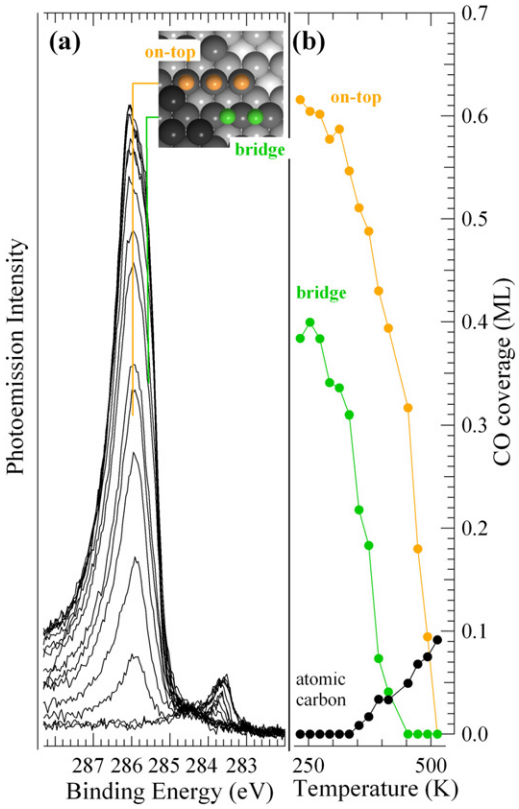

Figure 15. (a) Evolution of the C 1s core level spectra after annealing of the CO saturated layer prepared on the rhomboidal pyramids at different temperatures and quenching at 250 K. The peaks at 286 and 285.55 eV correspond to CO in on-top (orange) and bridge (green) sites, respectively. The component at about 283.6 eV is due to atomic carbon. The inset show possible inequivalent on-top and bridge adsorption sites. (b) Plot of the normalized C 1s intensity versus annealing temperature for a CO saturated layer prepared on the rhomboidal pyramids at $T = 200$ K relative to the CO species in on-top and bridge sites. Atomic carbon is shown in black.

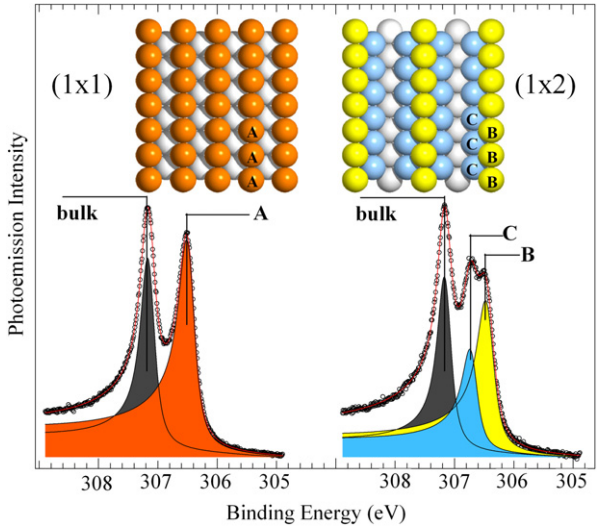

Figure 16. Rh $3d_{5/2}$ core level spectra from the (1×1) and (1×2) missing row reconstructed Rh(110) surfaces recorded at $T = 100$ K. Different colours in the top geometrical models (top) represent atoms with different coordination and geometrical arrangements: A—orange and B—yellow atoms ($n = 7$), C—blue atoms ($n = 9$).

atoms. Therefore the high reactivity of Rh nanopyramids towards CO dissociation is linked to the availability of under-coordinated Rh atoms, with CO molecules occupying preferentially on-top configurations, as schematically reported in figure 14 (bottom).

What turns out to be peculiar in the case of nanopyramids, with respect to the ripples morphology, is the very high density of kinked microfacets, produced by the steps running along [1–12], which provide a high density of low coordinated atoms (yellow $n = 5$ and orange $n = 6$ atoms in figure 14). The local atomic configuration of the microfacets, represents an open morphology (the nearest neighbour number is 6 with only one next nearest neighbour). With decreasing initial CO coverage, the density of free under-coordinated Rh atoms increases, which results in a higher fraction of dissociated CO. A comparison of different nanostructures shows that the reaction site for CO dissociation is the on-top configuration at the kinked step edges where Rh atoms have the lowest coordination.

In conclusion the possibility to form nanostructured surfaces with high density of low coordinated atoms, as for Rh(110), opens up the possibility to artificially increase the surface reactivity in a controlled way. In this respect core level spectroscopy can provide new insight into the elementary steps involved in the dynamics of molecular dissociation on surface defects: thanks to the high photon flux, the presence of different chemical and geometrically coordinated species can be accurately probed even when the populations are in the per cent range.

6. Thermal stability of reconstructed surfaces

By exploiting the brilliance of the x-ray radiation produced by synchrotron radiation facilities together with the energy tunability and high energy resolution, core level spectroscopy has developed into a time dependent method, thus allowing the evolution of surface processes to be followed on a timescale of seconds [105–107]. This data acquisition time is actually limited by different contributions arising from photon flux, transmission of electron energy analysers and electron detector efficiency.

An example of the application of the real-time surface core level shift measurements is the study of the thermal stability of metastable solid surfaces, such as the (1×1) Pt(100), which reverts to the hexagonal phase at temperatures above 390 K [108], and the (1×2) missing row Rh(110) reconstructed surface [109]. The latter, which can be obtained by hydrogen titration of the $(2 \times 2)p2mg$ oxygen structure, is thermodynamically unstable and converts into the (1×1) phase upon annealing.

In the (1×1)-Rh(110) phase, the Rh $3d_{5/2}$ spectrum reported in figure 16 shows a component with a core level shift of -675 meV (A-peak) relative to the bulk peak, while the spectrum of the (1×2) structure shows two surface components at -715 (B) and -445 meV (C), which are interpreted as due to first layer atoms and atoms in the (111) micro facets oriented

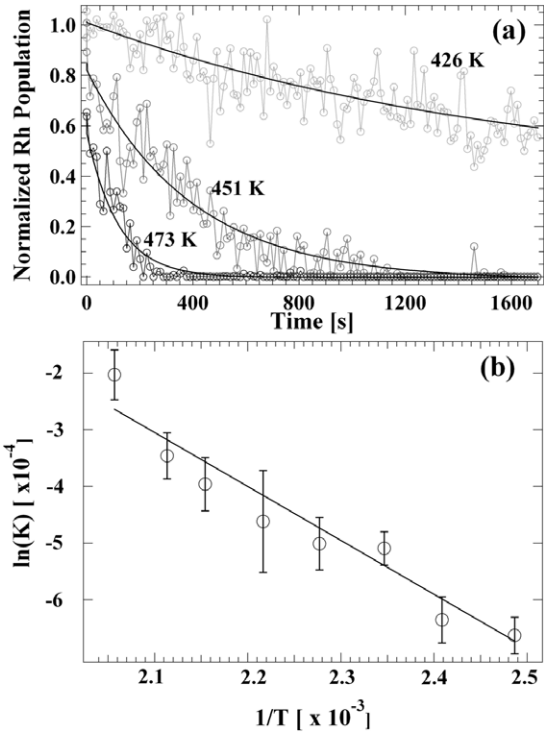

Figure 17. (a) Time evolution of the B-type Rh $3d_{5/2}$ surface core level shifted population (see figure 14) measured at different temperature. The curves are fitted using an exponential decay with constant $\tau = \nu \exp(-E_A/k_B T)$. (b) Arrhenius plot obtained by measuring the decay constant τ at eight different temperatures.

along the $[1\bar{1}0]$ troughs, respectively. Indeed the shift of the blue component is very close to the value found for the Rh(111) surface [110, 111]. DFT calculations yield results that are in very good agreement with these experimental findings.

In order to measure the activation energy for this surface transformation, the population of differently coordinated surface atoms at the surface was monitored as a function of time at different substrate temperatures. In particular the intensity of the B component, which is a fingerprint of the (1×2) structure, was characterized in detail.

Figure 17(a) shows some of the decay curves of the B component measured at different temperatures. The intensity decay has been fitted using the function $\Theta(t) = A \exp(-t\tau)$, with $\tau = \nu \exp(-E_A/k_B T)$ where E_A is the activation energy. By fitting the Arrhenius plot in figure 17(b) an activation energy $E_A = 0.95 \pm 0.13$ eV was extracted.

This value is in remarkable agreement with the activation energy for the (1×2) deconstruction process calculated on the basis of the climbing image nudged elastic band method, which takes into account the presence of surface defects [109].

The only mechanism which can quantitatively explain the experimental findings is the crumbling of the added atomic rows, ignited at a surface step (process A in figure 18, with and energy barrier of 1.14 eV), in agreement with STM experiments [112]. This step is followed by atomic diffusion along the missing row, as sketched in B in figure 18, a process with an activation barrier of 0.70 eV.

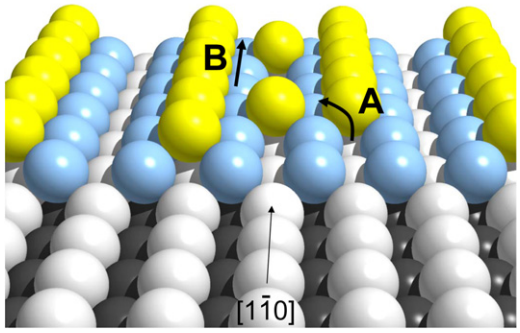

Figure 18. Schematic model of the deconstruction microscopic mechanism of the (1×2)-Rh(110) surface as obtained by DFT calculations. The atoms at the steps move via an exchange mechanism (A) into the troughs and subsequently diffuse (B) along the $[1\bar{1}0]$ direction.

These studies confirm the capability of core level spectroscopy to monitor the time and/or temporal evolution of surface processes which are confined exactly in the first atomic layer of a transition metal. This field of research can include the determination of the thermal stability of metal–oxide and oxide–oxide interfaces, the interdiffusion across the interface and the processes of interfacial segregation.

7. Bimetallic alloy surfaces: surface segregation during a chemical reaction

Alloy catalysts often display superior properties in terms of selectivity and reactivity with respect to catalysts based on pure monometallic materials. Rh and Pt are the main active components in catalysts used for the production of nitric acid via ammonia oxidation, widely used in the manufacture of nitrate fertilizers or in the production of N-containing products such as plastics and dyestuffs. The lifetime of these bimetallic catalysts is superior to that of monometallic Pt catalysts due to the suppression of self-poisoning by carbonaceous deposits.

PtRh catalysts are also used for the synthesis of hydrogen cyanide, usually via mixtures of NH_3, CH_4 and air and are the fundamental constituents of automotive three-way exhaust gas catalysts which have been used since 1983 [113–115]. The use of Pt and Rh in the automotive three-way catalysts is based on the fact that Pt is an excellent catalyst for oxidation of CO and hydrocarbons, while Rh is an efficient catalyst for NO reduction to N_2. Their performance strongly depends on the surface structure and composition of alloy particles, which is known to vary under different working conditions.

Model systems, such as single crystals in an UHV environment, can provide fundamental information about the properties of bimetallic catalysts and in particular about the adsorbate-induced modifications of the surface composition. In spite of the obvious technological interest, the determination of the first layer atomic population during a chemical reaction still remains a very demanding task. High surface sensitivity to the surface chemical composition of both adsorbed species and first layer atomic bimetallic elements has to be available on the same timescale of the surface reaction.

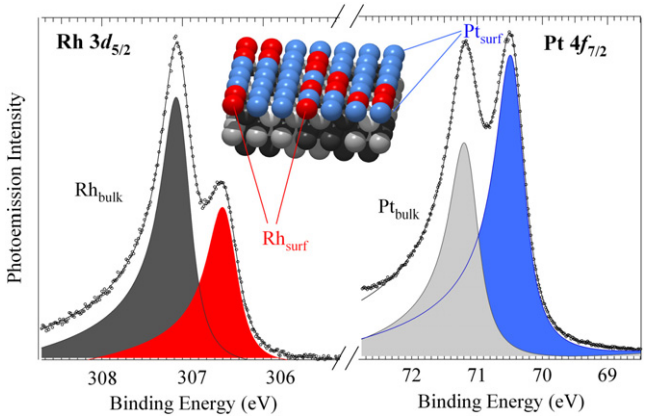

Figure 19. Rh $3d_{5/2}$ ($h\nu = 400$ eV) and Pt $4f_{7/2}$ ($h\nu = 200$ eV) core level spectra measured from the clean $Pt_{50}Rh_{50}(100)$ surface. In both spectra, the higher binding energy components correspond for both, Rh and Pt, to bulk atoms, while lower binding energy peaks originate from first layer atoms.

In this respect high energy resolution core level photoemission has been successfully applied for the determination of the population and the chemical configuration of $Pt_{50}Rh_{50}(100)$ first layer surface atoms, along with the corresponding variations in the sub-surface composition and the segregation process during a chemical reaction [116], all being key factors in determining the chemical properties.

As for the clean monometallic(100) surfaces, Pt $4f_{7/2}$ and Rh $3d_{5/2}$ core level spectra measured from the PtRh(100) surface present two components, as shown in figure 19. The higher binding energy peak is due to the bulk atoms, while the lower binding energy components, shifted by −705 (Pt) and −575 (Rh) meV from the corresponding bulk peaks, originate from first layer atoms. Chemically resolved STM images [117] with atomic resolution have indeed proved that no long range order exists on this surface and that only a limited tendency towards clustering takes place. Therefore the existence of sharp, well resolved core level components related to surface atoms is a clear indication that core level binding energies are not strongly affected by the different local chemical environment, but are mainly determined by electronic effects. Indeed it is the reduced coordination of surface atoms on the (100) surface which produces a d band narrowing at the surface, resulting in a surface component which is shifted to lower binding energies. A further chemical and geometrical contribution to the shifts can be understood by comparing the corresponding shift in the clean Pt(100) and Rh(100) surfaces. On Rh(100), without considering the contribution of the second layer which brings the shift to −600 meV [96], the SCLS is about −650 meV [41, 118]). On Pt(100) a recent investigation of the metastable (1 × 1) surface [108] reported a Pt $4f_{7/2}$ SCLS of −570 meV. This indicates that, while the absolute Rh $3d_{5/2}$ SCLS diminishes in the alloy surface, on Pt the effect is reversed. The major contribution to the shifts, excluding final state effects which have been found to play a minor role on Pt and Rh surfaces, is attributed to modified electronic properties of the surface atoms via ligand effects induced by the in-plane and second layer surface atoms nearest neighbours.

One of the most interesting outcomes of the surface core level shift measurements on bimetallic surfaces is the quantitative determination of the first layer composition. Indeed, using the relation $a_1 I_{Pts} + a_2 I_{Rhs} = 1$, where I_{Pts} and I_{Rhs} are the intensities of the Pt and Rh surface components, it is possible to determine the value of the a_1/a_2 ratio, which depends on photoemission cross sections, photoelectron kinetic energies and emission angles. This allows the evaluation of the surface composition as a function of time under different conditions such as surface temperature, adsorbate coverage, chemical composition and reaction time. The clean surface is found to be strongly Pt enriched (86%) in very good agreement with previous experimental findings [117, 119, 120] and with theoretical results, were a segregation energy of 0.25 eV/atoms has been found for a Pt impurity atom segregating in Rh [121].

Prior to the reactivity measurements, the oxygen (hydrogen)-induced Pt $4f_{7/2}$ and Rh $3d_{5/2}$ surface core level shifted components have been measured by O_2 (H_2) uptake experiments using a supersonic molecular beam [122]. These experiments revealed an unexpected Pt surface segregation for oxygen coverages below 0.3 ML (evaluated by monitoring the O 1s signal), while Rh segregation occurs only for larger oxygen exposures, when Rh atoms double coordinated with oxygen start to form, indicating that only above a critical coverage the higher O–Rh bond strength dominates over the reduction of surface energy per segregated Pt atoms.

Acquisition times down to 15 s/spectrum for Pt 4f, Rh 3d and O 1s core level spectra allow the surface and sub-surface composition to be monitored as a function of time while the $2H_2 + O_2 \rightarrow 2H_2O$ chemical reaction is going on, and water production in the gas phase is recorded simultaneously. Reaction cycles were made by exposing the sample to a constant hydrogen pressure, while modulating the oxygen flux with the shutter of the molecular beam, which allows reproduction of the gas exposure with high accuracy.

The variations of the clean and oxygen-induced surface components at 520 K, reported in figure 20, unambiguously show that Rh first layer depletion occurs also during the chemical reaction, as long as the surface coverage of oxygen remains below about 0.2 ML. The out-of-phase behaviour of the overall Pt and Rh surface population is also confirmed by the out-of-phase behaviour of Pt and Rh bulk populations, a clear fingerprint of the adsorbate-induced segregation phenomenon. Similar qualitative trends can be observed in a wide temperature range between 330 and 520 K, as reported in figure 21, with a Rh enrichment ranging from 14 to 31%. An interesting result is that such an increase in the Rh population cannot be obtained in a hydrogen ambient only. This was therefore tentatively explained by considering the contribution to surface segregation of another short lifetime surface species, such as OH.

This example demonstrates the value of the surface core level shift approach with its ability to distinguish between differently coordinated first layer metal species in a simple chemical reaction, even if the assignment of short-lived

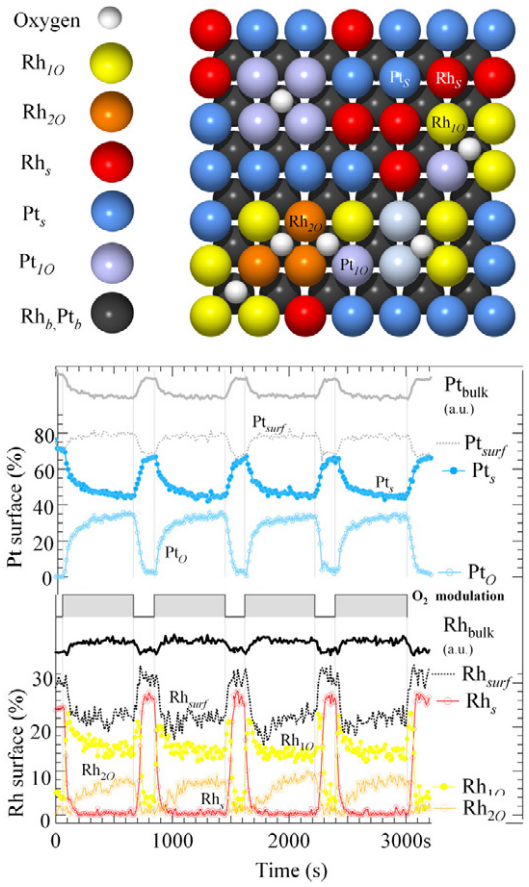

Figure 20. Time evolution of the clean and oxygen-induced Rh $3d_{5/2}$ and Pt $4f_{7/2}$ core level components, corresponding to the different chemical configurations sketched in the top model, measured during the $2H_2 + O_2 \rightarrow 2H_2O$ chemical reaction at $T = 520$ K from a PtRh(100) surface.

intermediate species remains somewhat speculative at the present time. An important technological imperative is to obtain a sufficient understanding of the properties of binary alloys which could permit optimization of the performance of bimetallic catalysts. We are, however, a long way from realizing this objective: core level spectroscopy will be one of the most helpful approaches to obtain an understanding of fundamental issues, such as the relationship between their geometric and electronic structure and the kinetics of adsorbate-induced surface segregation.

8. Outlook

In this review I have illustrated, with various examples, the strength that high energy resolution core level spectroscopy with synchrotron radiation has demonstrated in a wide range of systems, which can provide a valuable testing ground for the study of new, complicated surfaces. Indeed, many challenges still exist in this field. An important one is to expand the investigations to more complex systems such as nanostructured multicomponent alloys surfaces and nanoclusters, which are formed by small agglomerate of atoms, deposited on solid surfaces. The nature of these systems requires experimental techniques, such as core level spectroscopy, which can give information on a local scale. The unique and non-scalable thermodynamic, electronic, magnetic and structural properties which characterize these nanostructured atomic aggregates due to their highly reduced dimensions can be investigated by using core level spectroscopy. Although a broad range of phenomena has been studied in the last few years, in many cases a deeper insight was hampered by the lack of an adequate surface sensitivity and time resolution.

To this purpose, new electron energy analysers are currently under development [123], with the purpose of increasing electron detection efficiency, in particular using time-delay detectors. Up to two orders of magnitude higher detection sensitivity can be obtained which would allow us to reveal very small densities of surface atoms or to improve the data acquisition time, down to the limit of ms/spectrum range, where the finite transit time of electrons in the electron energy analysers becomes important. This, in combination with the use of supersonic molecular beams, will open new opportunities to probe fast and/or non-linear kinetic processes. The studies of intermediate species, which form when high pressure gas pulses impinge on the sample, or the study of the kinetics of thermally activated surface processes, by imposing a fast temperature perturbation on the system, will then both be possible. Perhaps the pulsed nature of synchrotron radiation is

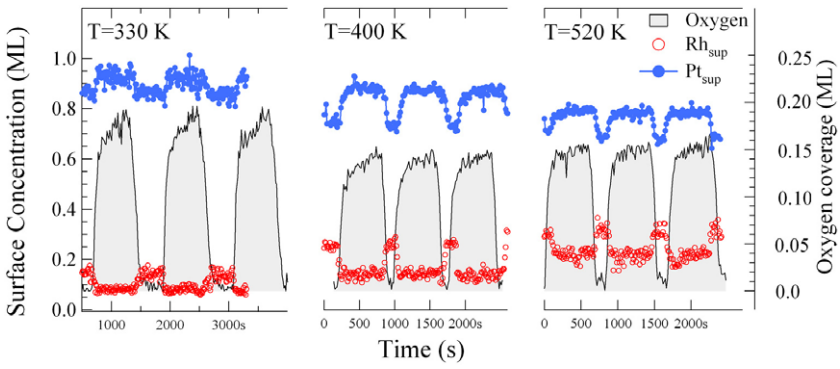

Figure 21. Time evolution of the Pt and Rh surface components at 330, 400 and 520 K during the $2H_2 + O_2 \rightarrow 2H_2O$ chemical reaction taking place on the PtRh(100). Oxygen coverage is shown as a grey curve.

an extraordinary opportunity to perform time-delayed pump–probe experiments to probe short-lived intermediate species in chemical reactions.

A new data acquisition time domain in the range of ms/spectrum will open the doors also to the investigation of self-sustained oscillatory chemical reactions which occur on many transition metal surfaces [124]. Furthermore, the advent of differentially pumped electrostatic lens systems [125] should make it possible to perform *in situ* studies of chemical reactions in the ms timescale at atmospheric pressure, an important step in the process of bridging the so-called 'pressure gap'. This new level of insights covering the complete range between UHV and ambient conditions can be achieved with coordinated team efforts using core level spectroscopy as part of a multi-method approach.

Certainly one of the most challenging and interesting future developments of core level spectroscopy would be to improve the experimental performance at high photoelectron kinetic energy ($E_{\mathrm{kin}} > 1000$ eV) [126]. This would be an important achievement to enhance the elemental bulk to surface sensitivity and to perform high energy resolution measurements in forward-scattering regime. Ultimately one would like to carry out investigations by probing the local chemical surface structure and composition in a time-resolved manner using photoelectron diffraction. The next generation of high brightness/ultrafast free-electron lasers, which is expected to explore the photon energy range up to that of hard x-rays, will probably allow this additional step. However the role of high photon flux in selectively producing chemical reactions via core or valence level excitations and the effects of radiation damage to samples in general is still not clear. The first moves in this direction have already shown that using stroboscopic techniques, it is possible to obtain a quantitative characterization of the interatomic potential energy surface of highly excited solids [127].

Finally, I want to mention the recent, remarkable progress of *ab initio* simulations based on density functional theory which widens the possibility of comparing with high accuracy experimental results and theoretical calculations: indeed the next generation of nanostructured solid surfaces will require an even closer collaboration between experimentalists and theoreticians in the field of core level photoelectron spectroscopy.

In spite of the progress made recently by various experimental methods, the best strategy to reach a deep understanding of surface structure and gas–surface interactions processes will undoubtedly remain, for many years to come, the combination of several experimental techniques, providing a wealth of complementary information: the unique capabilities of high energy resolution core level spectroscopy will naturally bring its contribution to new knowledge.

Acknowledgments

I would like to thank Silvano Lizzit and Giovanni Comelli with whom I have shared the experimental activity at the SuperESCA beamline and in the Surface Structure and Reactivity Laboratory at ELETTRA since 1994 for stimulating discussions, and their help and support.

I am indebted to all the scientists and friends who have taken an active part in the experiments presented in this review and in particular L Aballe, J N Andersen, F Bondino, F Buatier de Mongeot, L Bianchettin, M Kiskinova, A Locatelli, B E Nieuwenhuys, A Mikkelsen, T O Mentes, G Paolucci, L Petaccia, R Rosei, L Rumiz, U Valbusa, E Vesselli, J Weissenrieder and G Zampieri.

I am grateful to the theoreticians of the CNR-INFM-DEMOCRITOS National Simulation Centre in Trieste, who have been involved in the research work, in particular to S de Gironcoli for his invaluable contribution in the core level shift calculations and to S Baroni, C Sbraccia, N Bonini and M Peressi. K Honkala and J K Nørskov from the Centre for Atomic-scale Materials Physics at the Technical University of Denmark are also acknowledged. Kevin Prince is sincerely acknowledged for the critical reading of the manuscript. Special thanks go to J N Andersen for providing the data of figures 10 and 11.

Finally, I acknowledge the Sincrotrone Trieste S.C.p.A. and the Laboratorio TASC of INFM-CNR for providing beamtime and the laboratories where most of the presented research work was carried out.

References

[1] Egelhoff W F Jr 1986 *Surf. Sci. Rep.* **6** 253
[2] Rodriguez J A and Goodman D W 1992 *Science* **257** 897
[3] Woodruff D P and Delchar T A 1986 *Modern Techniques of Surface Science* vol 3 (Cambridge: Cambridge University Press)
[4] Lüth H 1997 *Surfaces and Interfaces of Solid Materials* (Berlin: Springer)
[5] Andersen J N and Almbladh C-O 2001 *J. Phys.: Condens. Matter* **13** 11267
[6] Baraldi A, Comelli G, Lizzit S, Kiskinova M and Paolucci G 2003 *Surf. Sci. Rep.* **49** 169
[7] Denecke R 2005 *Appl. Phys.* A **80** 977
[8] Andersen J N, Balasubramanian T, Almbladh C-O, Johansson L I and Nyholm R 2001 *Phys. Rev. Lett.* **86** 4398
[9] Hennig D, Methfessel M and Scheffler M 1994 *Surf. Sci.* **307–309** 933
[10] Andersen J N, Hennig D, Lundgren E, Methfessel M, Nyholm R and Scheffler M 1994 *Phys. Rev.* B **50** 17525
[11] Bagus P S, Illas F, Pacchioni G and Parmigiani F 1999 *J. Electron Spesctrosc. Relat. Phenom.* **100** 215
[12] Hardeveld R M, Schmidt A J G W, van Santen R A and Niemantsverdriet W 1997 *J. Vac. Sci. Technol.* A **15** 1642
[13] Hardeveld R M, Schmidt A J G W, van Santen R A and Niemantsverdriet W 1997 *J. Vac. Sci. Technol.* A **15** 1642
[14] Zaera F and Gopinath C S 2000 *Chem. Phys. Lett.* **332** 209
[15] Dore J E, Popp B N, Karl D M and Sansone F J 1998 *Nature* **396** 63
[16] Ma Z and Zaera F 2004 *Catal. Lett.* **96** 5
[17] Appleby A J and Foulkes F R 1989 *Fuel Cell Handbook* (New York: Van Nostrand Reinhold)
[18] Dudfiled C D, Chen R and Adock P L 2001 *Int. J. Hydrog. Energy* **26** 763
[19] Libuda J and Freund H-J 2005 *Surf. Sci. Rep.* **57** 157
[20] Libuda J 2005 *Surf. Sci. Rep.* **58** 755
[21] Madey T A, Yates Y T Jr and Erickson N E 1973 *Chem. Phys. Lett.* **19** 487
[22] Menzel D 1994 *Surf. Sci.* **299/300** 170

[23] Bradshaw A M, Menzel D and Steinkilberg M 1974 *Chem. Phys. Lett.* **28** 516
[24] Umbach E, Fuggle J C and Menzel D 1977 *J. Electron Spectrosc.* **10** 15
[25] Nilsson A and Mårtensson N 1989 *Solid State Commun.* **70** 923
[26] Nilsson A and Mårtensson N 1989 *Surf. Sci.* **211/212** 303
[27] Bjorneholm O, Nilsson A, Tillborg H, Bennich P, Sandell A, Hernnas B, Puglia C and Mårtensson N 1994 *Surf. Sci.* **315** L983
[28] Kinne M, Fuhrmann T, Whelan C M, Zhu J F, Denecke R and Steinrück H-P 2002 *J. Chem. Phys.* **117** 10852
[29] Surnev S, Sock M, Ramsey M G, Netzer F P, Wiklund M, Borg M and Andersen J N 2000 *Surf. Sci.* **470** 171
[30] Beutler A, Lundgren E, Nyholm R, Andersen J N, Setlik B J and Heskett D 1997 *Surf. Sci.* **371** 381
[31] Beutler A, Lundgren E, Nyholm R, Andersen J N, Setlik B J and Heskett D 1998 *Surf. Sci.* **396** 117
[32] Mårtensson N and Nilsson A 1995 *Applications of Synchrotron Radiation* (*Springer Series in Surface Science* vol 35) ed W Eberhardt (Berlin: Springer) p 65
[33] Lizzit S, Baraldi A, Cocco D, Comelli G, Paolucci P, Rosei R and Kiskinova M 1998 *Surf. Sci.* **410** 228
[34] Zhu F J, Kinne M, Fuhrmann T, Deneke R and Steinrück H P 2003 *Surf. Sci.* **529** 384
[35] Ganduglia-Pirovano M V, Scheffler M, Baraldi A, Lizzit S, Comelli G, Paolucci G and Rosei R 2001 *Phys. Rev.* B **63** 205415
[36] Baraldi A, Lizzit S and Paolucci G 2000 *Surf. Sci.* **457** L354
[37] Spanjaard D, Guillot C, Desjonqueres M P, Treglia G and Lecante J 1985 *Surf. Sci. Rep.* **5** 1
[38] Citrin P H, Wertheim G K and Baer Y 1983 *Phys. Rev.* **27** 3160
[39] Lundgren E, Mikkelsen A, Andersen J N, Kresse G, Schmid M and Varga P J 2006 *J. Phys.: Condens. Matter* **18** R481
[40] Baraldi A, Dhanak V R, Comelli G, Prince K C and Rosei R 1997 *Phys. Rev.* B **56** 10511
[41] Zacchigna M, Astaldi C, Prince K C, Sastry M, Comicioli C, Evans M and Rosei R 1996 *Phys. Rev.* B **54** 7713
[42] Doniach S and Šunjić M 1970 *J. Phys. C: Solid State Phys.* **3** 185
[43] Baraldi A, Lizzit S, Pohl K, Hofmann Ph and de Gironcoli S 2003 *Europhys. Lett.* **64** 364
[44] Wertheim G K, Riffe D M and Citrin P H 1994 *Phys. Rev.* B **49** 2277
[45] Wertheim G K, Riffe D M and Citrin P H 1989 *Phys. Rev. Lett.* **63** 1976
[46] Baraldi A, Dhanak V R, Comelli G, Prince K C and Rosei R 1996 *Phys. Rev.* B **53** 4073
[47] Oed W, Dotasch B, Hammer L, Heinz K and Müller K 1988 *Surf. Sci.* **207** 55
[48] Over H 1998 *Prog. Surf. Sci.* **58** 249
[49] Woodruff D P 2007 *Surf. Sci. Rep.* **62** 1
[50] Lizzit S, Pohl K, Baraldi S, Comelli G, Fritzsche V, Plummer E W, Stumpf R and Hofmann Ph 1998 *Phys. Rev. Lett.* **81** 3281
[51] Baraldi A, Lizzit S, Comelli G, Goldoni A, Hofmann Ph and Paolucci G 2000 *Phys. Rev.* B **61** 4534
[52] Lizzit S *et al* 2001 *Phys. Rev.* B **63** 205419
[53] Baraldi A, Lizzit S, Comelli G, Kiskinova M, Rosei R, Honkala K and Nørskov J K 2004 *Phys. Rev. Lett.* **93** 46101
[54] Ganduglia-Pirovano M V, Kudrnovsky J and Scheffler M 1997 *Phys. Rev. Lett.* **78** 1807
[55] Bianchettin L, Baraldi A, de Gironcoli S, Lizzit S, Petaccia L, Vesselli E, Comelli G and Rosei R 2006 *Phys. Rev.* B **74** 1
[56] Loffreda D, Simon D and Sautet P 1998 *J. Chem. Phys.* **108** 6447
[57] Hohenberg P and Cohn W 1964 *Phys. Rev.* B **136** 864
[58] Kohn W and Sham L 1965 *Phys. Rev.* A **140** 1133
[59] Perdew J P and Sunger A 1981 *Phys. Rev.* B **23** 5048
[60] Ceperley D and Alder B 1980 *Phys. Rev. Lett.* **45** 566
[61] Baroni S, de Gironcoli S, dal Corso A and Giannozzi P http://www.quantum-espresso.org
[62] Kiskinova M 1991 *Poisoning and Promotion in Catalysis Based on Surface Science Concepts and Experiments* (New York: Elsevier Science)
[63] Kiskinova M 1988 *Surf. Sci. Rep.* **8** 359
[64] Goodman D W 1984 *Heterogeneous Catalysis, IUCCP Conf.* ed B Shapiro (College Station, TX: Texas A&M University)
[65] Peen C H F and Goodman D W 1984 *Proc. Symp. on the Surface Science of Catalysis* (*Symp. Ser. Am. Chem. Soc.* vol 288) ed M L Devinny and J L Gland (Washington, DC: ACS) p 185
[66] Kiskinova M and Goodman D W 1981 *Surf. Sci.* **108** 64
[67] Goodman D W and Kiskinova M 1981 *Surf. Sci.* **105** L265
[68] Goodman D W 1996 *J. Chem. Phys.* **100** 13090
[69] Feibelmann P J and Hamann D R 1984 *Phys. Rev. Lett.* **52** 61
[70] Feibelmann P J 1990 *Phys. Rev.* B **3** 9452
[71] Blealy K and Hu P 1999 *J. Am. Chem. Soc.* **121** 7644
[72] Zhang C J, Hu P and Lee M-H 1999 *Surf. Sci.* **432** 305
[73] Lynch M and Hu P 2000 *Surf. Sci.* **458** 1
[74] McAllister B and Hu P 2005 *J. Chem. Phys.* **122** 8470
[75] Bianchettin L, Baraldi A, Vesselli E, de Gironcoli S, Lizzit S, Petaccia L, Comelli G and Rosei R 2007 *J. Phys. Chem.* C **111** 4003
[76] Vesselli E, Baraldi A, Bondino F, Comelli G, Peressi M and Rosei R 2004 *Phys. Rev.* B **70** 115404
[77] Weststrate C J, Baraldi A, Rumiz L, Lizzit S, Comelli G and Rosei R 2004 *Surf. Sci.* **566–568** 486
[78] Barth J V 2000 *Surf. Sci. Rep.* **40** 75
[79] Christmann K 1999 *Surf. Sci. Rep.* **9** 1
[80] Sustorovich E and Sellers H 1998 *Surf. Sci. Rep.* **31** 1
[81] Sustorovich E 1986 *Surf. Sci. Rep.* **6** 1
[82] Carlisle C I, King D A, Bocquet M-L, Cerdà J and Sautet P 2000 *Phys. Rev. Lett.* **84** 3899
[83] Lundgren E, Kresse G, Klein C, Borg M, Andersen J N, De Santis M, Gauthier Y, Konvicka C, Schmid M and Varga P 2002 *Phys. Rev. Lett.* **88** 246103
[84] Over H, Kim Y D, Seitsonen A P, Wendt S, Lundgren E, Schmid M, Varga P, Morgante A and Ertl G 2000 *Science* **287** 1474
[85] Gustafson J *et al* 2005 *Phys. Rev.* B **71** 115442
[86] Gustafson J *et al* 2004 *Phys. Rev.* B **92** 46101
[87] Zambelli T, Wintterlin J, Trost J and Ertl G 1996 *Science* **273** 1688
[88] Hammer B and Nørskov J K 2000 *Adv. Catal.* **45** 71
[89] Hammer B, Morikawa Y and Nørskov J K 1996 *Phys. Rev. Lett.* **76** 2141
[90] Vang R T, Honkala K, Dahl S, Vestergaard E K, Schnadt J, Lægsgaard E, Clausen B S, Nørskov J K and Besenbacher F 2005 *Nat. Mater.* **4** 160
[91] Gambardella P, Sljivancanin Z, Hammer B, Blanc M, Kuhnke K and Kern K 2001 *Phys. Rev. Lett.* **87** 56103
[92] Kyuno K and Ehrlich G 1998 *Phys. Rev. Lett.* **81** 5592
[93] Gustafson J, Borg M, Mikkelsen A, Gorovikov S, Lundgren E and Andersen J N 2003 *Phys. Rev. Lett.* **91** 56102
[94] Silvestri W, Graham A P and Toennies J P 1998 *Phys. Rev. Lett.* **81** 1034
[95] Tromp R M and Toennies J P 1998 *Phys. Rev. Lett.* **81** 1050
[96] Baraldi A, Bianchettin L, Vesselli E, de Gironcoli S, Lizzit S, Petaccia L, Zampieri G, Comelli G and Rosei R 2007 *New J. Phys.* **9** 143
[97] Zhang Y, Jacobs G, Sparks D E, Dry M E and Davis B H 2002 *Catal. Today* **71** 411

[98] Zubkov T, Morgan G A Jr and Yates J T Jr 2002 *Chem. Phys. Lett.* **362** 181
[99] Somorjai G A 1994 *Introduction to Surface Chemistry and Catalysis* (New York: Wiley)
[100] Liu Z-P and Hu P 2003 *J. Am. Chem. Soc.* **125** 1958
[101] Molle A, Buatier de Mongeot F, Molinari A, Fuerkaiti F, Boragno C and Valbusa U 2004 *Phys. Rev. Lett.* **93** 256103
[102] Molle A, Buatier de Mongeot F, Molinari A, Boragno C and Valbusa U 2006 *Phys. Rev.* B **73** 155418
[103] Buatier de Mongeot F, Toma A, Molle A, Lizzit S, Petaccia L and Baraldi A 2006 *Phys. Rev. Lett.* **97** 56103
[104] Buatier de Mongeot F, Toma A, Molle A, Lizzit S, Petaccia L and Baraldi A 2007 *Nanoscale Res. Lett.* **6** 251
[105] Baraldi A, Barnaba M, Brena B, Cocco D, Comelli G, Lizzit S, Paolucci G and Rosei R 1995 *J. Electron. Spectrosc. Relat. Phenom.* **76** 145
[106] Baraldi A, Comelli G, Lizzit S, Kiskinova M and Paolucci G 2003 *Surf. Sci. Rep.* **49** 169
[107] Denecke R, Kinne M, Whelan C M and Steinrück H-P 2002 *Surf. Rev. Lett.* **9** 797
[108] Baraldi A *et al* 2007 *J. Chem. Phys.* **127** 164702
[109] Baraldi A, Lizzit S, Bondino F, Comelli G, Rosei R, Sbraccia C, Bonini N, Baroni S, Mikkelsen A and Andersen J N 2005 *Phys. Rev.* B **72** 75417
[110] Baraldi A, Lizzit S, Novello A, Comelli G and Rosei R 2003 *Phys. Rev.* B **67** 205404
[111] Andersen J N, Hennig D, Lundgren E, Methfessel M, Nyholm R and Scheffler M 1994 *Phys. Rev.* B **50** 17525
[112] Africh C, Esch F, Comelli G and Rosei R 2002 *J. Chem. Phys.* **116** 7200
[113] Nieuwenhuys B E 1999 *Adv. Catal.* **44** 259
[114] Nieuwenhuys B E, Siera J, Tanaka K I and Hirano H 1994 *Environmental Catalysis* (*ACS Symposium Series* vol 552) (Washington, DC: ACS)
[115] Nieuwenhuys B E 1996 *Surf. Rev. Lett.* **3** 1869
[116] Baraldi A *et al* 2005 *J. Am. Chem. Soc.* **127** 5671
[117] Wouda P T, Nieuwenhuys B E, Schmid M and Varga P 1996 *Surf. Sci.* **359** 17
[118] Baraldi A, Comelli A, Lizzit S, Rosei R and Paolucci G 2000 *Phys. Rev.* B **61** 12713
[119] Ren D, Qin J H, Wang J B and Tsong T T 1993 *Phys. Rev.* B **47** 3944
[120] Siera J, van delft F C M J M, Langeveld A D and Nieuwenhuys B E 1992 *Surf. Sci.* **264** 435
[121] Christensen A, Ruban A V, Stolte P, Jacobsen K W, Skriver H L, Norskov J K and Besenbacher F 1997 *Phys. Rev.* B **56** 5822
[122] Baraldi A, Rumiz L, Moretuzzo M, Barnaba M, Comelli G, Lizzit S, Paolucci G, Rosei R, Buatier de Mongeot F and Valbusa U 2002 *J. Vac. Sci. Technol.* A **20** 683
[123] Lacovig P, Sala A, Gardonio S, Baraldi A and Lizzit S 2008 in preparation
[124] Imbihl R and Ertl G 1995 *Chem. Rev.* **95** 697
[125] Bluhm H, Hävecker M, Knop-Gericke A, Kleimenov E, Schlögl R, Teschner D, Bukhtiyarov V I, Ogletree D F and Salmeron M 2004 *J. Phys. Chem.* B **108** 14340
[126] Panaccione G *et al* 2006 *Nucl. Instrum. Methods* B **246** 106
[127] Fritz D M *et al* 2007 *Science* **315** 633